Engineering Geology xxx (xxxx) 106256

Contents lists available at ScienceDirect

Engineering Geology

journal homepage: www.elsevier.com/locate/enggeo

Experimental analysis of desiccation cracks on a clayey silt from a large-scale test in natural conditions

Josbel A. Cordero [a], Pere C. Prat [a, *], Alberto Ledesma [a, b]

[a] Dept. of Civil and Environmental Engineering, UPC-BarcelonaTech, Spain
[b] Int. Centre for Numerical Methods in Engineering, CIMNE, Barcelona, Spain

ARTICLE INFO

Keywords:
Soil drying
Soil cracking
Field test
Clayey silt
Soil-air interface

ABSTRACT

This paper presents an experimental investigation on the impact of environmental variables on soil cracking in natural conditions. The test was performed on a large soil specimen of initial size 3 × 3 × 0.5 m exposed to real atmospheric conditions during one year, to include different seasonal weather conditions. The specimen was instrumented to monitor and record the main variables within the soil (temperature, volumetric water content, suction) and others at the soil-air interface (wind speed and direction, temperature, relative humidity, solar radiation, rain intensity). The experiment extends previous experience from laboratory desiccating tests in two main aspects: the size of the specimen and the exposition to a natural environment. A large size is desirable to reduce the effect of the mechanical boundary conditions. Conducting the test in a natural setting allows including variables that cannot be properly studied in laboratory conditions such as solar radiation or wind velocity, which this research has shown to constitute two key factors controlling water evaporation and eventually soil cracking. The soil-air interface constitutes a narrow zone with high gradients of most of the variables involved controlling the fluxes of water and energy. The experiment has shown that variation of those gradients has considerable implications in soil cracking.

1. Introduction

Cracking in desiccating soils is a topic receiving much attention in recent research due to its relevance in regions subjected to periodic droughts or in many engineering and agricultural applications. The study of cracking as a hazard is pursued in a diversity of scientific fields such as applied mathematics, physics, biology, planetary science, earth science or soil science, and in engineering (civil, mining, chemical or mechanical). Although until recent years this study has been limited, the new scenario of global climate change has contributed to develop interest and knowledge on this issue, since soil cracking has a significant impact in the performance of the ground, affecting both surface and underground infrastructure (Amarasiri et al., 2011; Cordero et al., 2017; Costa et al., 2013; Gui and Zhao, 2015; Kodikara et al., 2004; Lakshmikantha et al., 2009; Levatti et al., 2017; Lozada et al., 2019; Nahlawi and Kodikara, 2006; Péron et al., 2009; Sánchez et al., 2014; Stirling et al., 2017; Tang et al., 2020; Trabelsi et al., 2012; Wang et al., 2018; Yesiller et al., 2000; Yoshida and Adachi, 2004). However, soil cracking prediction is still an open problem in need of a fundamental solution. The lack of a model to provide insight into the nature of crack initiation and crack path instabilities demand the development of a theory with a wide range of applicability, based on experimental, numerical, and theoretical efforts.

Cracking in soils usually appears as a result of desiccation processes that occur following changes of environmental conditions, which strongly influence the hydraulic and mechanical behaviour of the material. The interaction between the atmosphere and the soil plays a major role in such desiccation-cracking phenomena. Clayey soils under severe environmental conditions, and repetitive shrink/swell processes, are vulnerable to the formation of desiccation cracks (Harris, 2004; Neal et al., 1968). Environmental variables such as wind velocity, air relative humidity or solar radiation have a strong influence on the evaporation and infiltration of water through the soil surface which, in addition to soil properties and mechanical boundary conditions, define the evolution and patterns of desiccation cracks (Blight, 1997; Cui et al., 2005; Shokri et al., 2015). Some aspects of this topic, such as closing of existing cracks or changing of the crack pattern after alternating dry-wet periods, have not been investigated in detail so far, perhaps because of the complexity of the analysis from a coupled hydro-mechanical point of view.

* Corresponding author.
E-mail addresses: josbel.andreina.cordero@upc.edu (J.A. Cordero), pere.prat@upc.edu (P.C. Prat), alberto.ledesma@upc.edu (A. Ledesma).

https://doi.org/10.1016/j.enggeo.2021.106256
Received 17 August 2020; Received in revised form 25 February 2021; Accepted 29 June 2021

Many researchers have studied the evolution of desiccation cracks using small-size specimens in the laboratory (Corte and Higashi, 1960; Costa et al., 2013; Lakshmikantha et al., 2018; Miller et al., 1998; Nahlawi and Kodikara, 2006; Péron et al., 2009; Rodríguez et al., 2007; Sánchez et al., 2013; Shin and Santamarina, 2011; Tang et al., 2011; Tollenaar et al., 2018; Wang et al., 2018). These laboratory results are fundamental for the understanding of the conditions in which cracks develop. However, they also show that the size of the specimen as well as the mechanical boundary conditions imposed by the containers used to form the specimens have a large impact in the process of crack formation and propagation, and in the structure of the crack pattern that appears on the surface of the material (Cuadrado, 2019; Cuadrado et al., 2019; Lakshmikantha et al., 2012; Lakshmikantha et al., 2018).

The impact of the mechanical boundary conditions in laboratory tests seems to be less for larger specimens (Cuadrado et al., 2021; Lakshmikantha et al., 2018), thus suggesting that to study soil cracking in natural field conditions the experiments should be conducted, ideally, in as large as possible specimens. In the field, very large areas of soil may become affected by cracking with little or no impact of the existing mechanical boundary conditions, which rarely are well defined and have an effect only in a very little portion of all soil mass involved. Unfortunately, this type of field or large-size tests are scarce (Cui et al., 2013; Konrad and Ayad, 1997; Li and Zhang, 2011; Stirling et al., 2018; Stirling et al., 2020; Yesiller et al., 2000; Yu et al., 2021).

In general, tests conducted in the laboratory on specimens (even large ones) are rarely representative of field conditions, and such experiments struggle to account for heterogeneity as observed in real natural conditions. Additionally, laboratory experiments (conducted in the laboratory atmosphere or in environmental chambers) cannot replicate well the environmental conditions found in natural settings. Recent research (Cordero, 2019) has shown that drying of a soil is much more efficient in the field than in an environmental chamber, even with a significantly smaller relative humidity in the latter. Of course, this cannot be explained solely with the different relative humidity and size of the specimens: there are other physical variables which play a significant role in the field experiment that are difficult to reproduce faithfully in the laboratory, such as the solar radiation or wind velocity, despite the efforts made in this regard (Davarzani et al., 2014; Tristancho et al., 2012; Yamanaka et al., 1997). For instance, in the field, the wind removes water vapor and changes the environmental boundary condition at the soil-air interface while the solar radiation provides energy for evaporation. In the laboratory these physical variables are very difficult to apply, and the use of devices such as lamps or blowers for that purpose result in a behaviour which is different from the one in natural conditions (Cuadrado et al., 2021; Levatti, 2015; Levatti et al., 2019).

Nevertheless, the understanding of cracking in natural field conditions is particularly important in research applications to geotechnical infrastructure, and the study of mechanisms of crack initiation and development under natural atmospheric conditions is of substantial practical value. When comparing cracking experiments carried out in laboratory conditions with measurements of cracking in the field, it becomes evident that the variables indicated above play a fundamental role in this phenomenon, which complicates any comparison in quantitative terms (Cordero et al., 2016; Lakshmikantha, 2009; Ledesma, 2016). That reason justifies the development of desiccation tests in the field, conducted on in-situ soils under atmospheric conditions, that would be more realistic for engineering applications. In such full-scale in-situ tests, however, the boundary conditions (especially the hydraulic) might be difficult to monitor and control. Instrumentation, as well, would be more complicated and some measurements might become impossible: for example, the global gravimetric water content measured from weight changes could not be obtained.

As a first step toward the objectives described in the previous paragraphs, this paper presents the description and the results of an experiment designed to study the impact of environmental variables (wind velocity, air relative humidity, solar radiation, temperature) on soil cracking in natural conditions. The test was performed on a large soil specimen of initial size 3 × 3 × 0.5 m, cast into a high-density polyethylene container and exposed to real atmospheric conditions during one year to include different seasonal weather conditions. The specimen was fully instrumented for air and soil mass and surface temperatures, air and soil relative humidity, heat flux in the soil, matrix suction, volumetric water content, electrical conductivity, vapor pressure, wind speed and direction, global solar radiation, and continuously recording of the global weight of the specimen, thus allowing the measurement of the changes of the gravimetric water content due to evaporation and rainfall.

2. Material and methods

2.1. Soil used in the investigation

The experiment was conducted at the UPC–BarcelonaTech Agròpolis site in Viladecans (Catalonia-Spain), which is a scientific-technical unit providing services to several research groups. It is located near the Barcelona-El Prat international airport in an area surrounded by farms and crops. The soil used in the test was taken from stacked natural material left from the excavation (approximately 3 m deep) of the foundation of the main building in the site, near the placement of the test installations. At first glance, this is a coarse-grained soil with a fine matrix and enough plasticity, prone to cracking when desiccated. Only the fraction with particles smaller than 2mm was used for the test.

The soil is a clayey silt with almost 10% of clay and a substantial amount of silt and sand. However, the geotechnical classification according to the Unified Soil Classification System (USCS) characterizes this soil as low plasticity clay (CL). A compilation of data and information about the physical, mechanical, and hydraulic properties of the Agròpolis soil can be found in Cordero (2019). Table 1summarizes the values of the relevant parameters of the soil used in the test, and the specimen state conditions at test initiation.

2.2. Specimen preparation

The preparation of the soil specimen required a rigorous program to obtain material as homogeneous as possible. In preparation for the test, the natural soil was first sequentially sieved in the field, using three sieves of apertures 40, 20 and 2mm. After that, the sieved soil was mixed with plain water in a concrete mixer truck to make a slurry with an initial moisture content of approximately 43.5%, 1.5 times the soil's liquid limit (28.9%). Using a gutter from the mixer, the resulting slurry was poured into the test container filling the container's volume (4.5 m^3) completely and resulting in a fairly homogeneous specimen.

Table 1
Summary of material soil properties.

Soil property	Experimental value
Specific gravity of solid particles	2.70
Specific surface area (particles <2 mm)	44 m^2/g
Organic matter content	2.44%
Liquid limit, w_L	28.9%
Plastic limit, w_P	16.5%
Shrinkage limit, w_R	13.8%
Sand content	48.3%
Silt content	42.1%
Clay content	9.6%
Compressibility index, C_c	0.12
Initial gravimetric water content, w_{ini}	43.53%
Initial natural unit weight, γ_{ini}	17.46 kN/m^3
Initial dry unit weight, $\gamma_{d,\ ini}$	12.16 kN/m^3
Initial void ratio, e_{ini}	1.2

To prevent vegetation growth during the test, an herbicide (GOAL Supreme®) was applied during placement of the slurry into the container. During the one-year cycle of the test no vegetation growth took place. Determination of the Atterberg limits with and without the herbicide showed that its addition did not change their value.

Fig. 1shows the specimen immediately after pouring the slurry in the container. Fig. 2 shows a detail of the specimen at test initiation, with its surface flush with the container's upper borders. At that time there was no water film at the surface.

2.3. Experimental set-up

The experiment began on 2015-01-17T11:00Z, during the 2014–15 winter season, and lasted for one year. Representation of dates and times in this paper uses standard ISO 8601.

The soil specimen was cast into the 3 × 3 × 0.5 m container that was previously placed on a steel structure made of IPN200 profiles, attached with especial couplings to four load cells resting on a reinforced concrete foundation slab capable of supporting the weight of the ensemble (see Fig. 1) without differential settlements. These load cells were used to record the change of the specimen's weight, which allowed calculating the variation of the gravimetric moisture content and estimate the rate of evaporation.

To monitor the main physical variables involved in the cracking process the specimen was externally (Figs. 1–2) and internally (Fig. 3) instrumented with several types of sensors designed to record variables relative to the soil, the air, and the soil-air interface. Some of the variables that could not be measured at the test site were obtained from a weather station of the Catalan Weather Service, located 1.5 km from the test site. All sensors used in the experiment are described in detail in Table 2. Before pouring the slurry, a geotextile was placed covering the container's bottom surface and the internal sensors were mounted on supports attached to the container (Fig. 3). Finally, water was added in order to saturate the geotextile.

A camera was located with unobstructed view of the specimen's surface inside a box, which served as protection from the weather (see Fig.

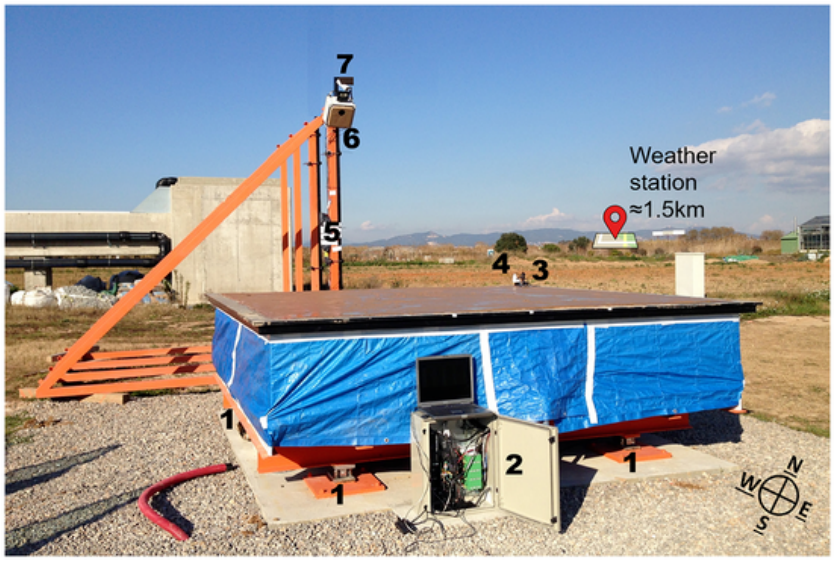

Fig. 1. Overview of the field test: 1) steel structure, load cells and coupling; 2) data recording system; 3) anemometer; 4) two VP3 sensors to measure relative humidity, temperature and vapor pressure; 5) support structure; 6) digital camera; 7) IR120 infrared remote temperature sensor.

Fig. 2. Detail showing some of the external sensors and the initial conditions of the test, with the specimen's surface flush with the container's upper borders and no water film at the surface.

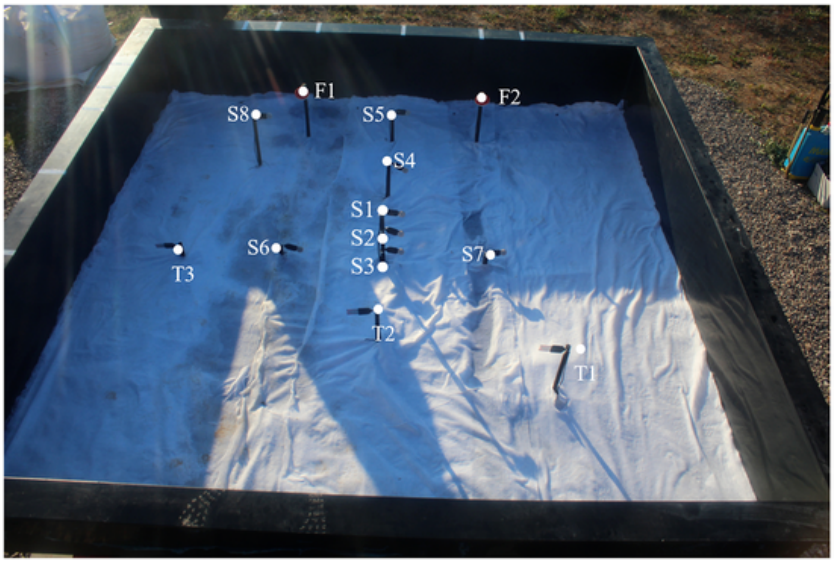

Fig. 3. Distribution of the internal sensors: (T1-T3) Volumetric water content, temperature and electric conductivity; (S1-S8) matrix suction; (F1-F2) soil heat flux.

1). The position of the camera with respect to the experiment was such that it did not cause a preferential shadow, path of dripping or runoff. Because of that, the position could not be zenithal, affecting the direct measurement of the images captured during the monitoring. Therefore, to quantify surface measurements of the crack patterns using an image analysis method it became necessary, previous to the image analysis, to correct each photo to the zenithal position. For this purpose, a routine was developed in MATLAB that allowed to implement the image rectification for the subsequent image analysis.

3. Experimental results

Based on weather conditions, several periods have been defined as "dry" and "wet". A "dry period" in this context means a period of significant duration with no rainfall events registered. A "wet period" is a period with rainfall events that may include some interleaved short-time lapses without rain. Consecutive dry and wet periods define the "dry-wet cycles". During the one-year duration of this experiment, 13 dry-wet cycles were identified (Table 3). In this analysis, the lengths of the dry and wet periods are arbitrary, with the goal of having a maximum of three dry-wet cycles each meteorological season. The shortest dry period is one day, and the shortest wet period is two days, both during the first dry-wet cycle.

Fig. 4 shows the average daily water volume influx calculated from weight changes for each dry and wet period. In this paper, soil water content increases are positive while decreases are negative. There are some negative values that represent daily evaporation, which was less during wet periods than during dry periods. High positive values were obtained when the rainfall resulted in significant weight increments in a short time period, such as during the wet period of cycle 6.

3.1. Initial behaviour

Fig. 5 shows the variation of the water amount in the specimen by direct measurement through weight changes, and rainfall from the weather station during the first 19 days of the experiment. The first episode of rain occurred on the day after test initiation with a total rainfall of 7.3 mm in two days. The average intensity during this event was 0.365 mm/h with a maximum of 1 mm/h. Although at times the rain caused increments of total weight, the specimen lost moisture during the episode.

Shortly after test initiation, a water film began to accumulate on the surface as shown in Fig. 6. The increasing thickness of the water film (that reached a maximum of 1 cm) triggered some spills alongside the upper container edges, with a resulting water loss that cannot be considered evaporation, but is evident in the pronounced slope of the weight loss during the first 30 h of the test, before the first rainfall event (see Fig. 5). During that period, the soil particles in the slurry settled by gravity with water migrating to the surface, forming the water film and increasing the moisture content near the surface.

During the first three days of the experiment (the first dry-wet cycle), the specimen's surface experienced an estimated average settlement of approximately 3 cm. Part of the rainwater was retained above the soil surface in the container's space freed by the specimen's settlement (Fig. 7). Settlement continued for some time afterwards, with a final average measured value of 12 cm.

Estimation of the water volume influx from the experiment is needed to evaluate the water amount in the soil. This volume influx was obtained from the measurements of the specimen weight/mass changes during one-hour intervals; hence the incremental volume influx may be calculated using Eq. (1) where it is estimated that 1 mm of water is equivalent to 1 kg/m^2, assuming a water density of 1000 kg/m^3 and a constant evaporation surface of $A = 9$ m^2:

$$\dot{E} = \frac{\dot{M}}{A\rho_w} \tag{1}$$

where $\dot{M}$ is the rate of mass loss in kg/h and $\dot{E}$ is the volume influx in m/h. The term $\dot{E}$ is considered positive if it represents an increase of the soil water content. The volume influx is a direct measurement of evaporation if no rainfall occurs during the observation period (such as in dry periods).

The average settlement of the soil mass can be directly computed from the specimen's weight change if the soil remains saturated. If not, it is possible to estimate that value by using the global gravimetric water content, w, obtained from the continuous measurement of the specimen's weight and the average volumetric water content, θ, measured locally by the sensors installed within the soil mass. Eq. (2) can be used for that purpose:

$$\Delta H = H_0 - H_t \approx \frac{\Delta V}{A} \approx \frac{\Delta\left(\frac{w \bullet W_{sol}}{\theta \bullet \gamma_w}\right)}{A} \tag{2}$$

where ΔH is the soil height increment, H_0 is the initial height, H_t is the height at time "t", V is the total soil volume, W_{sol} is the weight of the solid particles and γ_w is the unit weight of water. The average settlement

Table 2
Sensors installed to monitor the different variables.

Loc	Variables	Sensor (*)	Range	Units	Accuracy / Comment
1.5 km from test site	Rainfall	Pluviometer	0–200	mm	Weather station from the Catalan Weather Service (*Servei Meteorològic de Catalunya*)
	Wind speed	Anemometer and vane	0–55	m/s	
	Wind direction		0–360	°	
	Global solar radiation	Pyranometer	0–1400	W/m^2	
	Air temperature	Thermistor	-30 to +46	°C	
	Relative humidity	Capacitive hygrometer	0–100	%	
External (Fig. 1)	Weight changes	Load cells 350i Utilcell (1)	0.5–5000	kg	3000 divisions O.I.M.L. R60 class C
	Relative Humidity	VP3 Decagon (3)	0–100	%	Accuracy depends on humidity and temperature (DecagonDevices, 2015)
	Air temperature		−40 to +80	°C	
	Vapor Pressure		0–47	kPa	
	Wind speed	Davis cup anemometer (4)	0–58	m/s	±5%
	Wind direction		0–360	°	±7°
	Surface temperature	IR120 Campbell thermometer (7)	−25 to +60	°C	±0.2 °C
Internal (Fig. 3)	Volumetric water content	5TE Decagon (T1-T3)	0–100	%	±3%
	Soil temperature		−40 to +50	°C	±1 °C
	Electrical conductivity		0–23	dS/m	±10%
	Matrix suction	MPS6 Decagon (S1-S8)	−9 to −100,000 (pF 2.00–9.01)	kPa	±10%
	Soil heat flux	HFP01SC Hukseflux (F1-F2)	−2000 to +2000	W/m^2	±3%

(*) Labels in parenthesis indicate the sensor shown in the corresponding figure.

Table 3
Dry-wet cycles identified during the one-year period.

Cycle	Begin dry date	Begin wet date	Total days
1	2015-01-17	2015-01-18	3
2	2015-01-20	2015-01-30	16
3	2015-02-05	2015-02-17	28
4	2015-03-05	2015-03-13	21
5	2015-03-26	2015-04-15	32
6	2015-04-27	2015-05-19	24
7	2015-05-21	2015-06-11	34
8	2015-06-24	2015-07-24	59
9	2015-08-22	2015-09-01	22
10	2015-09-13	2015-09-23	31
11	2015-10-14	2015-10-20	26
12	2015-11-09	2015-12-05	48
13	2015-12-27	2016-01-04	21
End	2016-01-17	Total days	365

(ΔH) after the first dry-wet cycle was estimated between 2 and 3 cm, from Eq. (2). Note that in that equation settlement and volume reduction are positive.

In Eqs. (1) and (2) the evaporation from the soil surface is essentially a one-dimensional vertical process. This is clearly the case at least before cracks are formed, but the equations are assumed to be also reasonable after cracks develop. The validity of this assumption is discussed below.

During the first 19 days of the experiment there were two rainfall events with one longer dry period in between (see Fig. 5). The evaporation rate became more regular (after the first cycle) and less abrupt after the first day when water was lost by spilling over the container walls, in addition to evaporation. Although the thickness of the water film varied with rain, spilling did not happen again during the remainder of the experiment. In particular, water slowly evaporated during the 10-day dry period between the first and second rainfall events. At the same time, the specimen continued reducing its thickness even without an evident crack pattern on the surface and only small edge cracks (Fig. 8).

The second rainfall event (Fig. 9) was slightly more intense than the first one, with a total rainfall of 7.4 mm during a period of six days, an average intensity of 0.673 mm/h and a maximum of 1.9 mm/h.

3.2. Implications for soil cracking

Immediately after filling the container, some narrow millimetric cracks appeared randomly at locations governed by the prevalent heterogeneity near the container walls (Fig. 10). These cracks faded as the water began to accumulate at the specimen's surface (see Fig. 6). Eventually, on day 22 after test initiation (early February), some permanent cracks began forming and defining a pattern which was captured by the camera monitoring the surface of the specimen. Fig. 11 shows the pattern of cracks in development, with a thin water film still remaining on the surface at the corners of the container indicating that the specimen was mostly saturated. This confirms that, in restrained conditions, cracks may appear even if the soil is saturated, as claimed in earlier research (Chertkov, 2002; Konrad and Ayad, 1997). In this case, the first cracks appeared at the centre of the container where no water was visible at the soil surface and therefore the soil was, perhaps, not fully saturated locally. Note that very close to saturation some suction may still develop as represented in a typical Soil Water Characteristic Curve for clayey soils. Thus, cracks may initiate very close to saturation, depending on the mechanical boundary conditions and the soil defects (Lakshmikantha et al., 2018; Shin and Santamarina, 2011). The global gravimetric water content of the soil at the onset of crack opening was about 35% (see Fig. 12a), and the estimated average crack width was approximately 1 cm. Note that at crack initiation the water content was well above the liquid limit (28.9%).

The extent of cracking during the complete one-year duration of the experiment is presented in Fig. 13 in terms of surface variations using CIF, the area of cracks relative to the total nominal area (Miller et al., 1998), as a descriptor. Rainfall is also shown in the same figure to relate cracking to the natural wetting and drying cycles. The CIF values were estimated before and after each rainfall interval. Fig. 14 shows the surface crack pattern at eight significant times during the test: (a) at test initiation, (b) at crack initiation and the start of the first significant CIF increase, (c) at the end of winter when a slower rate of crack propagation began, (d) at the end of spring, during the period of slow crack propagation rate, (e) late summer, at the beginning of the second significant CIF increase, (f) at the end of summer during the CIF increase, (g) at mid-autumn when the maximum CIF was measured, and (h) at early winter, close to the end of the experiment. Each image is cross-referenced in Fig. 13, to visualize the time the pictures were taken and the value of the CIF at that instant.

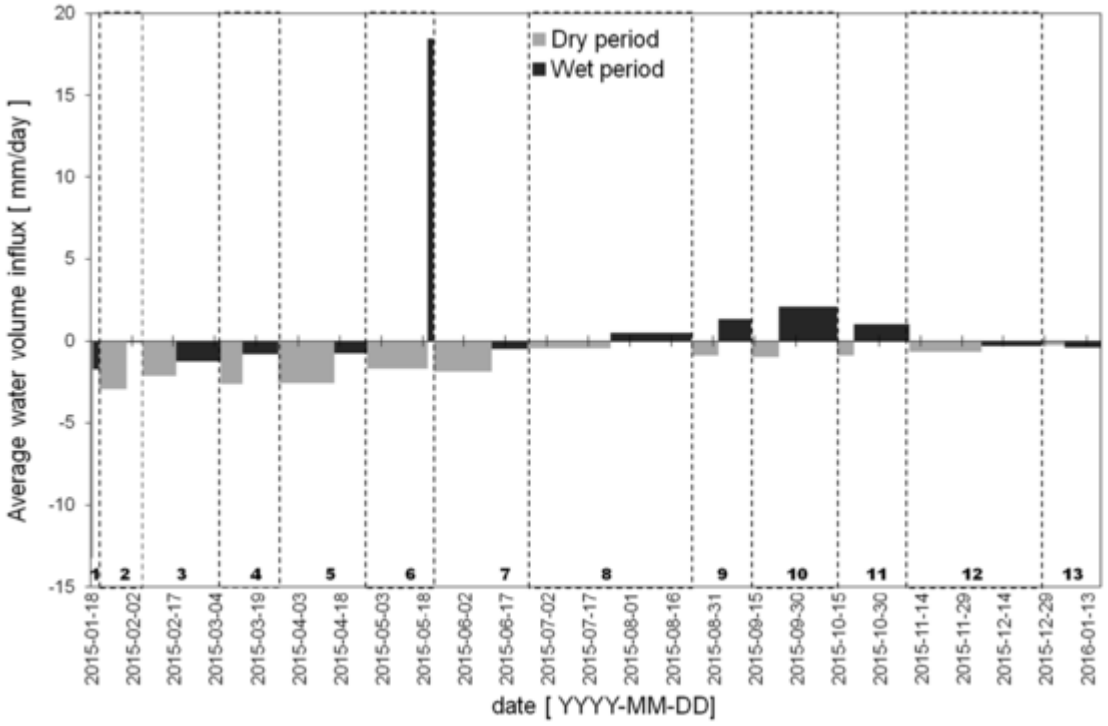

Fig. 4. Average water volume influx computed for each dry and wet periods of each dry-wet cycle.

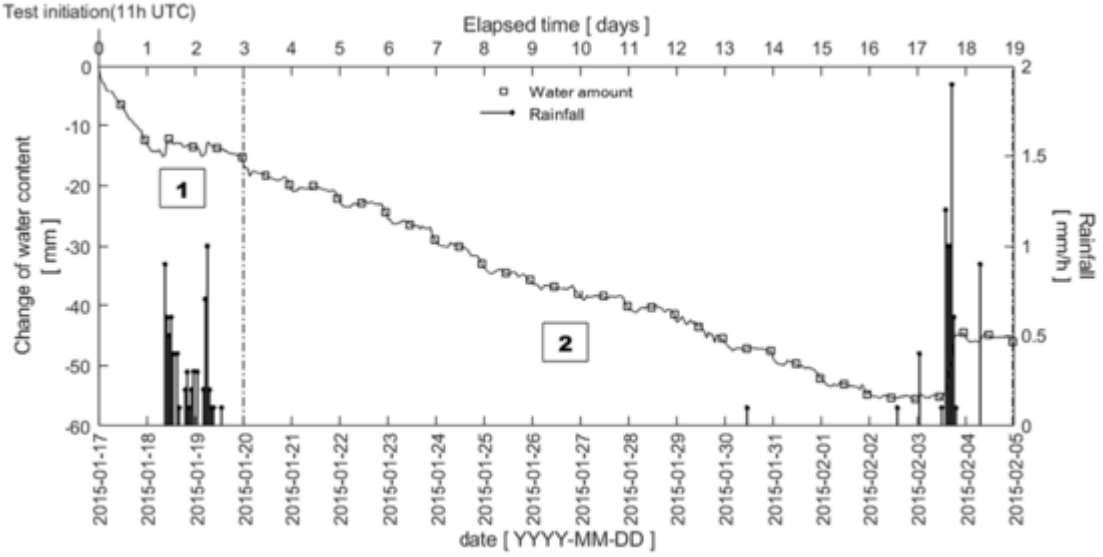

Fig. 5. Change of water content by direct measurement of weight changes, and rainfall from the weather station during the first 19 days of the experiment (in mm of water).

Fig. 6. Specimen surface two hours after test initiation.

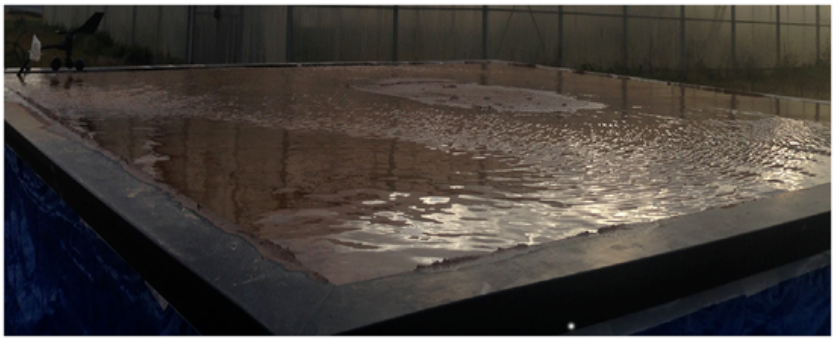

Fig. 7. Specimen surface at the end of the first rainfall event (day 3 after test initiation).

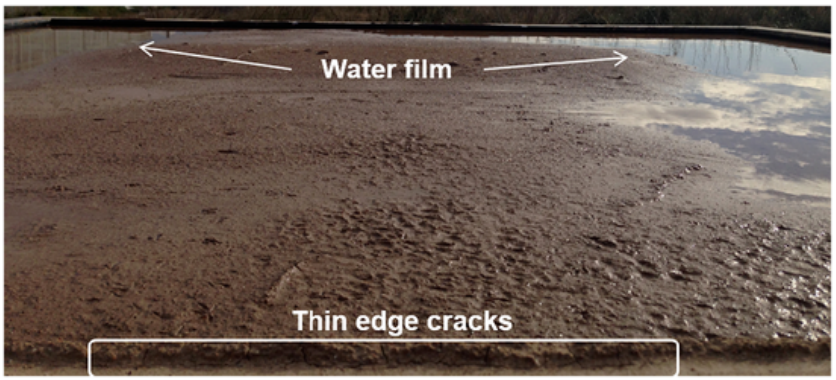

Fig. 8. Specimen surface after 10 days without rainfall (day 13).

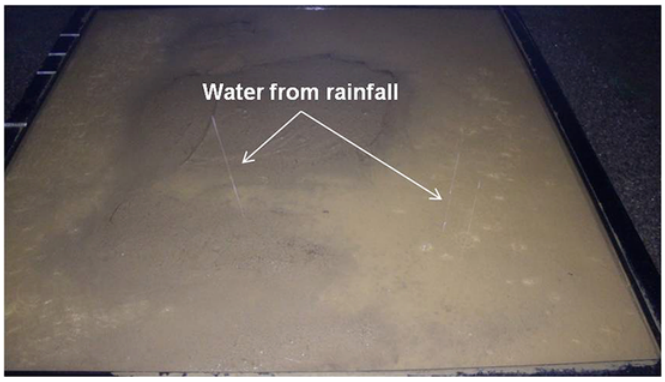

Fig. 9. Specimen surface during the second rainfall event (day 18).

Fig. 13 shows that after crack initiation (Fig. 14b), the CIF increased rapidly from 0% to 12% during winter (Fig. 14c). From late winter to late summer, the CIF increased at a much slower rate (Fig. 14d) to approximately 15% in late summer (Fig. 14e). From late summer to mid-autumn, the total area of cracks increased significantly (Fig. 14f), with the CIF reaching a maximum of almost 30% (Fig. 14g), as a reaction to rainfall events in early autumn. In that period, the larger cracks became wider as a consequence of the water retained in the existing cracks. Later, when the specimen became again drier, the CIF decreased because small local failures of the edges of the larger cracks (similar to failure of a vertical cut) resulted in loose material filling the existing cracks, thus reducing their area. By the end of autumn, the CIF value increased again (Fig. 14h), with a final value of approximately 25% after the one-year duration of the experiment.

Fig. 13 shows two significant CIF increases, one in winter from 0 to 12% after the initial four dry-wet cycles; and the other from late summer to mid-autumn approximately from 15% to 30%. The first CIF increment is due to a conventional desiccation process and a subsequent soil shrinkage. Note that there is no water available from any water

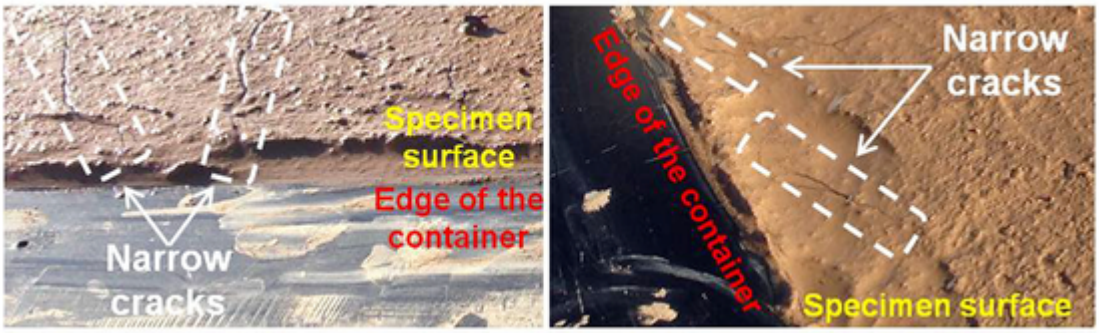

Fig. 10. Thin cracks formed close to the lateral walls of the container at the start of the test.

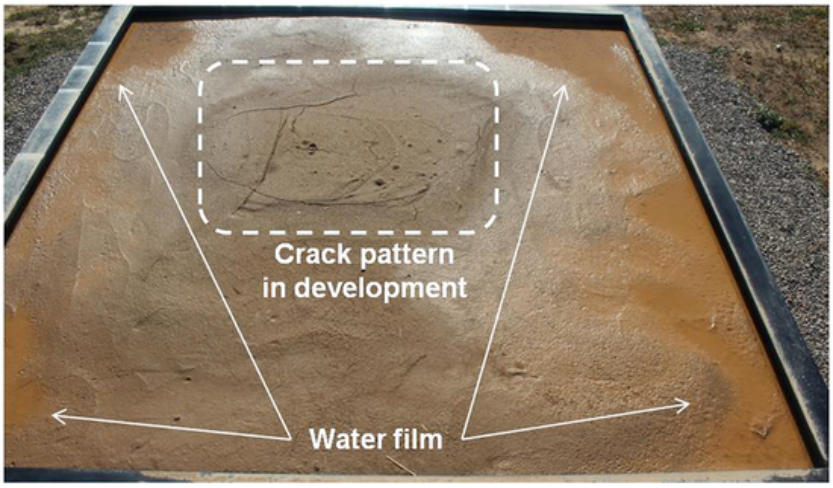

Fig. 11. Specimen surface 24 days after test initiation.

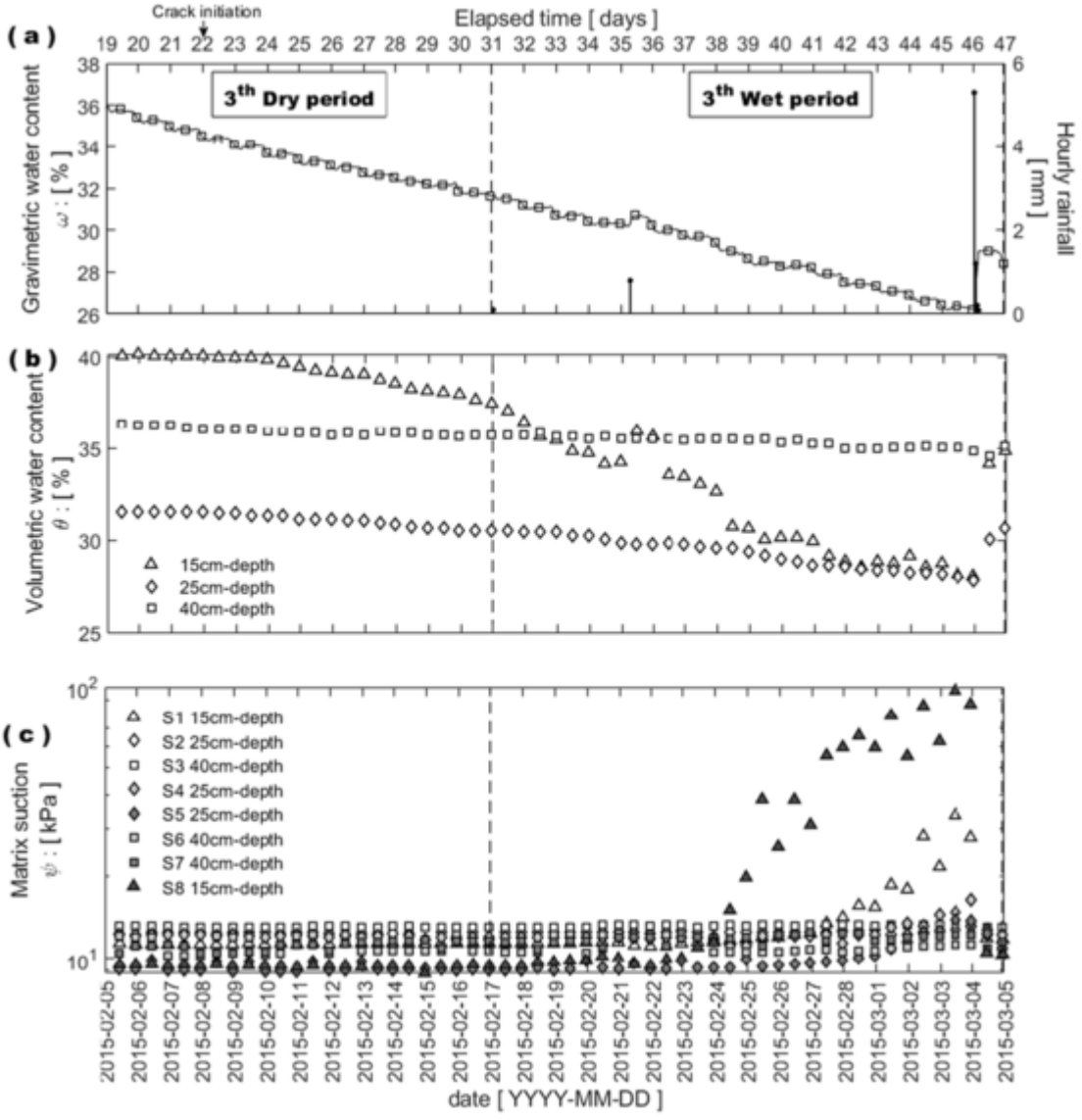

Fig. 12. Data corresponding to the third dry-wet cycle: (a) variation of the gravimetric water content; (b) volumetric water content from 5TE Decagon sensors; (c) matrix suction from MPS6 Decagon sensors at different locations.

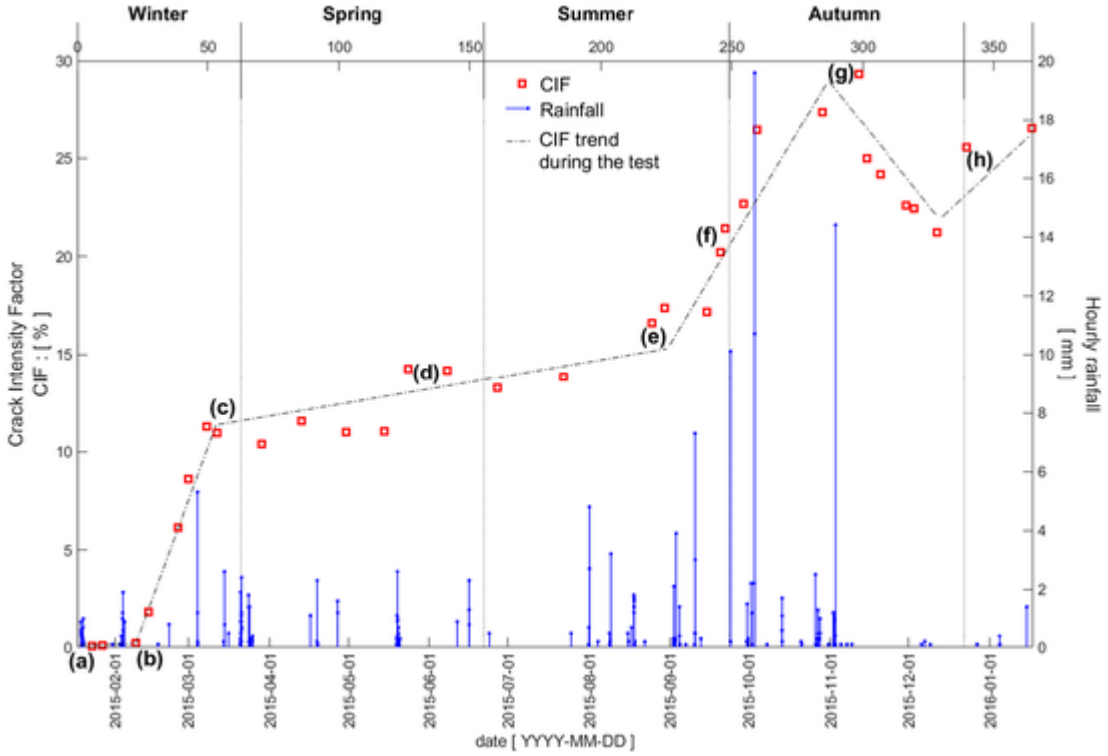

Fig. 13. Evolution of the crack intensity factor (CIF) during the experiment, compared to precipitation. Labels (a-h) refer to the images in Fig. 14.

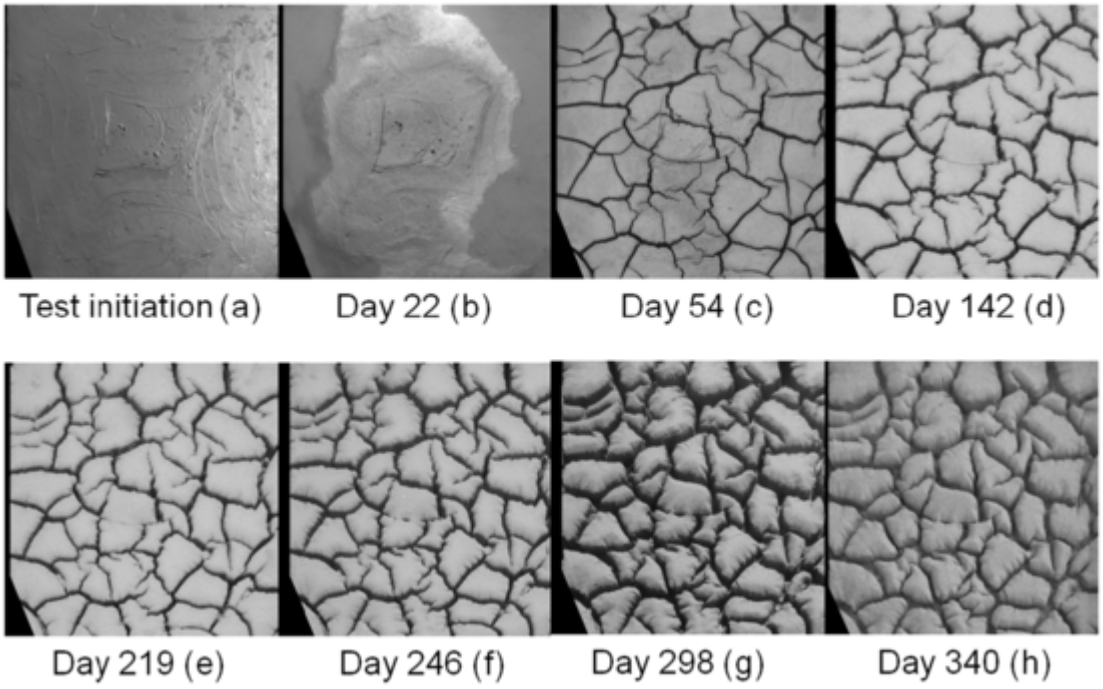

Fig. 14. Evolution of the crack pattern during the test.

table to provide moisture. In addition to that, rainfall during that period was too small to compensate evaporation, as it will be described later. The second CIF increment is due to another mechanism, since during late summer soil suction was high and the crack pattern was well defined already. High intensity rainfalls in autumn increased the water content producing two simultaneous effects, a small swelling of the soil mass and a fast drop of suction which reduced the unsaturated soil strength. Most of the crack edges collapsed as they were unstable when suction was reduced, thus creating new thinner cracks behind. Overall, this process increased CIF up to a point in which the collapsed edges filled the initial thicker cracks and eventually reduced the CIF during late autumn.

3.3. Volumetric water content, suction and electrical conductivity

Besides using the change of weight of the specimen to evaluate the global change of the water content, readings from several sensors were

used to locally measure variables such as the volumetric water content, matrix suction, or electric conductivity.

Fig. 12 shows the evolution of some measured variables (global gravimetric water content, local volumetric water content and suction) between days 19 and 47. The initial volumetric water content shown in Fig. 12b, suggests that moisture distribution is not homogeneous within the soil mass. In fact, the slurry poured in the container experienced sedimentation and self-weight consolidation. In this type of processes void ratio and water content are homogeneous at the beginning, but they decrease with depth over time (Bonin et al., 2019). In this experiment the initial volumetric water content was between 42% and 43%, but after a few hours the distribution depicted in Fig. 12b was measured. Note that water content at the deepest sensor was higher than expected; this is attributed to the geotextile installed at the bottom of the container that was fully saturated before pouring the slurry.

Crack initiation adjusts well with the decreasing of volumetric water content in the upper layer of the specimen (upper 15 cm). However, the increment of the measured suction lags several days with respect to the start of the water loss process (see Figs. 12b,c). Note that tensiometers S8 and S1 are closer to the surface and react to the desiccation process at day 38 and 41 respectively. The different readings from both tensiometers are due to a crack that developed close to tensiometer S8 and that may lead to different measurements in sensors located at the same depth. Indeed, sensors in the soil mass may constitute a preferential point for crack initiation or propagation.

Fig. 15 shows that the contours of higher water content advance vertically toward the bottom of the specimen once a visible crack pattern starts developing at the surface with CIF above 10% (near day 50), which indicates that the drying front gradually moves vertically downwards toward the bottom of the specimen. The contour lines are densely distributed near the surface suggesting a significant loss of water (about 42% on day 3, and 30% by the time cracking started). On the contrary, in the lower layer, the contour lines are more spaced indicating that the same moisture content remains longer.

Approximately after day 80 of the test, when the cracks were deeper and wider, there were daily oscillations between day and night of about 1% to 2% of the volumetric water content. The volumetric water content tends to increase during rainfall events. Peaks of volumetric water content reflect the rise of measured values, which are more evident in the upper layer sensors while readings at the lower layers' sensors appear unaffected. The increments of the values of the volumetric water content due to rain presented a delay of between 5 and 12 h with respect to the rainfall event. In the case of evaporation, the volumetric water content at the upper layer decreased at a higher rate than at the lower layers, which seemed to lose less water.

To help understanding the changes of the volumetric water content, vertical profiles at selected days during each season are presented in Fig. 16. In the upper layer (sensors located at 15 cm depth), the change of the volumetric water content happened faster during winter when the test started (Fig. 16a). During that season, the volumetric water content at depth 15 decreased from 42% to 24%, suggesting a transition in the drying process as the volumetric water content profile changed its trend. The evaporation mode changed from one-dimensional (vertical), to three-dimensional, horizontal and vertical (Li and Zhang, 2011). First the water from the soil evaporates only from the soil surface, with a vertical flow direction. Later, when cracks have formed, the pattern of water flow due to evaporation may change. This is a controversial issue, as some authors report a rapid decrease of water content, especially after the falling-rate evaporation stage (Song, 2014), whereas some works suggest that the evaporation rate after primary cracking does not change substantially (Lakshmikantha, 2009; Tang et al., 2011). A recent work (Cuadrado, 2019) suggests that the atmosphere inside a crack is different from the external environment and evaporation through crack walls is rather limited (or it is delayed with respect to the water exchange on the soil's top surface).

The volumetric water content profile obtained on 2015-04-29 (grey triangles in Fig. 16b) shows an anomalous trend in the upper measurement, with a moisture gain. This can be attributed to the lack of direct evaporation during two days when the surface of the specimen was covered with special panels for external calibration tests of a reflectometer (Alonso-Arroyo et al., 2015).

During summer (Fig. 16c) the volumetric water content changed little. Only some moderate rainfall events (between 3 and 5 mm/h) caused slight changes of the measurements recorded at the upper layer. In fact, during summer (period 8 in Fig. 4) the total water volume influx was almost nil, as rainfall compensated the evaporation in that period. Most of the profiles corresponding to autumn (Fig. 16d) are incomplete

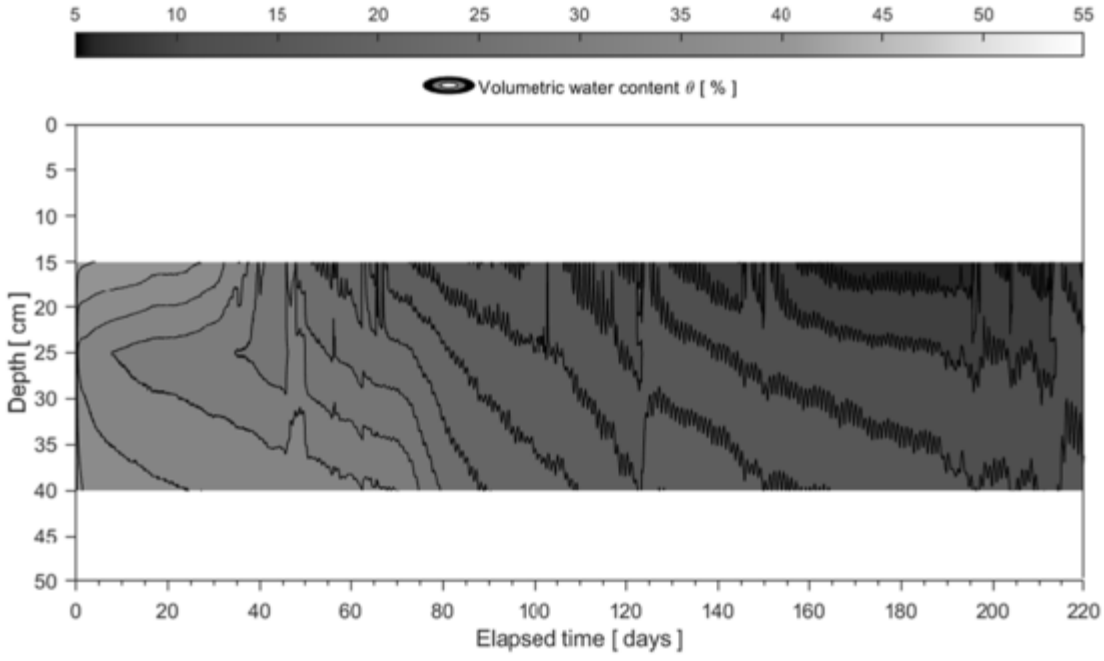

Fig. 15. Contour map of volumetric water content. Sensors stopped measuring continuously after day 220.

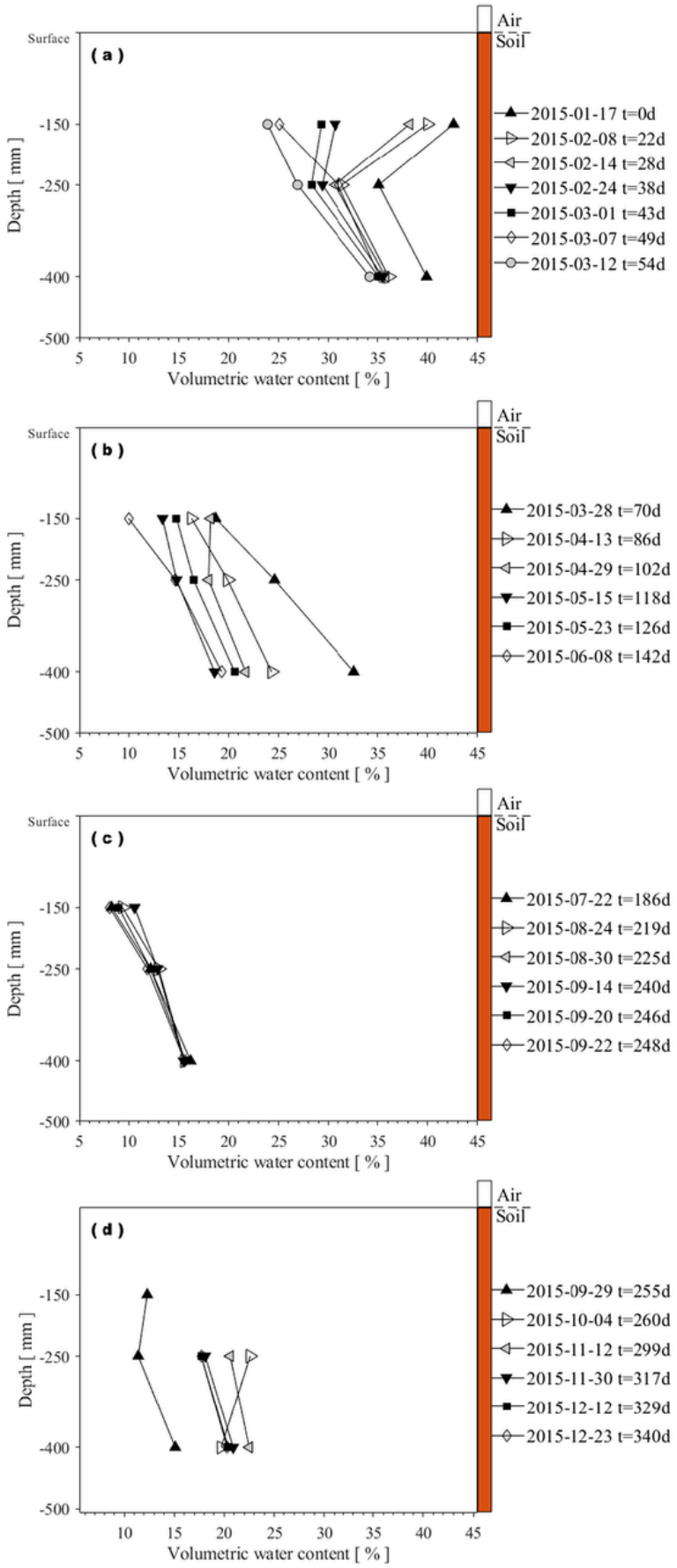
(a)
Surface
Air
Soil
Depth [mm]
-150
-250
-400
-500
5
10
15
20
25
30
35
40
45
Volumetric water content [%]
2015-01-17 t=0d
2015-02-08 t=22d
2015-02-14 t=28d
2015-02-24 t=38d
2015-03-01 t=43d
2015-03-07 t=49d
2015-03-12 t=54d
(b)
2015-03-28 t=70d
2015-04-13 t=86d
2015-04-29 t=102d
2015-05-15 t=118d
2015-05-23 t=126d
2015-06-08 t=142d
(c)
2015-07-22 t=186d
2015-08-24 t=219d
2015-08-30 t=225d
2015-09-14 t=240d
2015-09-20 t=246d
2015-09-22 t=248d
(d)
2015-09-29 t=255d
2015-10-04 t=260d
2015-11-12 t=299d
2015-11-30 t=317d
2015-12-12 t=329d
2015-12-23 t=340d

Fig. 16. Profiles of volumetric water content at selected days: (a) winter; (b) spring; (c) summer; (d) autumn; $t = 0$ corresponds to 6 h after test initiation.

because the sensor at the upper layer stopped recording measurements from October, when heavy rainfall with intensity of 20 mm/h flooded the specimen. This flooding also caused the middle layer to become more wet because of cracking-induced preferential paths for water flow (day 260 in Fig. 16d).

The simultaneous measurements of suction and volumetric water content provide data to determine the soil water retention curve at multiple depths, as shown in Fig. 17. The water retention curves at the middle and bottom layers are different than the curve at the upper layer, probably because of the variation of soil density with depth, and also because of the development of surface desiccation cracks. Solid circles in Fig. 17 represent the soil water retention curve from laboratory data, which started with a void ratio similar to the field test. The difference among curves can be attributed to porosity changes during the desiccation process.

The results show that suction in general decreases with depth and increases with time, except during a rainfall event. Because of the measurement technique of the sensors, there is a slight delay for water to infiltrate the soil around the ceramic disk in the sensor. This caused the suction changes lagging some time behind the rainfall. However, suction changes during wet periods happened faster than changes during dry periods. The matrix suction increased more in spring than in winter. The values of suction at the upper layer reached almost 300 kPa in winter, while in spring suction reached approximately 10 MPa. The tensiometers stopped working after reaching that value.

Measurements from the sensors located closest to the surface (15 cm deep) allow detecting desaturation which occurs after day 28 (2015-02-14). At that time, the CIF and volumetric water content were approximately 4% and 38% respectively. The matrix suction for the middle and bottom layers (sensors at 25 and 40 cm depth, respectively) delayed reporting desaturation probably because the surrounding soil was denser due to the rearrangement experienced during the process of water expulsion during self-weight consolidation. However, because of the development of drying cracks at the surface the relationship between water content and suction at the upper layer is quite different than the one at the deeper layers (Song et al., 2016).

The electrical conductivity of the water used for the field test was 1.2 dS·m^{-1} on average. This value could possibly be affected by the herbicide used with the soil-water mixture. The evolution of the specimen's electrical conductivity was monitored at three depths. At test initiation, the sensors registered a decrease of electrical conductivity with depth from 1.5 to 1.3 dS·m^{-1}. As the soil dried, the values decreased because of the salts left by the evaporating water and the corresponding loss of ion mobility, showing that the electrical conductivity in the soil varies with the water content.

Fig. 18 shows that the electrical conductivity decreased with depth in the period before the surface cracks appeared (first 22 days of the test), when the gravimetric water content had fallen below 35%. This is likely because the average water content also decreased when the water was flowing from the bottom to the upper layer as a consequence of evaporation at the latter. However, Fig. 19 shows that the electrical conductivity in terms of the local water content does not depend on depth. Probably the structure and porosity of the soil surrounding the sensors alter the ion mobility, thus affecting the electrical conductivity values. The sensor in the upper layer registered an electrical conductivity drop at a volumetric water content approximately 42% (close to the initiation of cracking).

The geometrical features of the cracks affect the evolution of the electrical conductivity. As an example, the crack depth decreases considerably the electrical conductivity and with an increase in the number of cracks, the electrical conductivity depends much more on geometric crack features such as depth, length, and width (Kong et al., 2012).

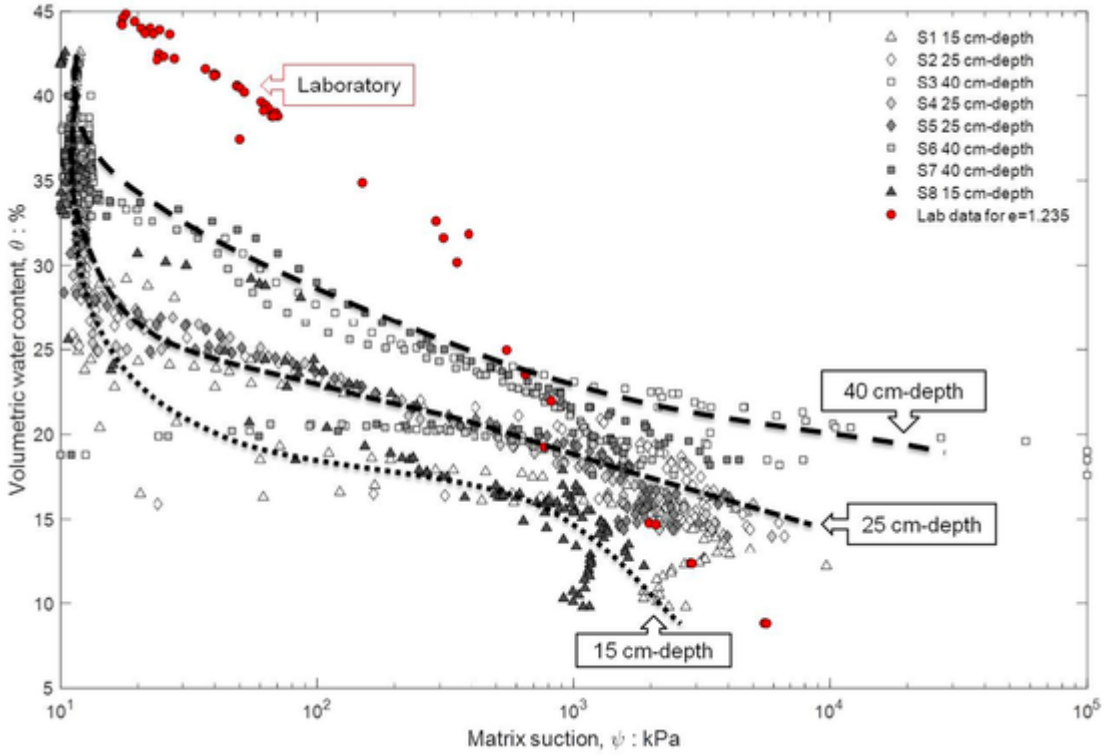

Fig. 17. Soil water retention curve obtained from the field test since initiation until 2015-06-12 and from tensiometer and hygrometer in the laboratory.

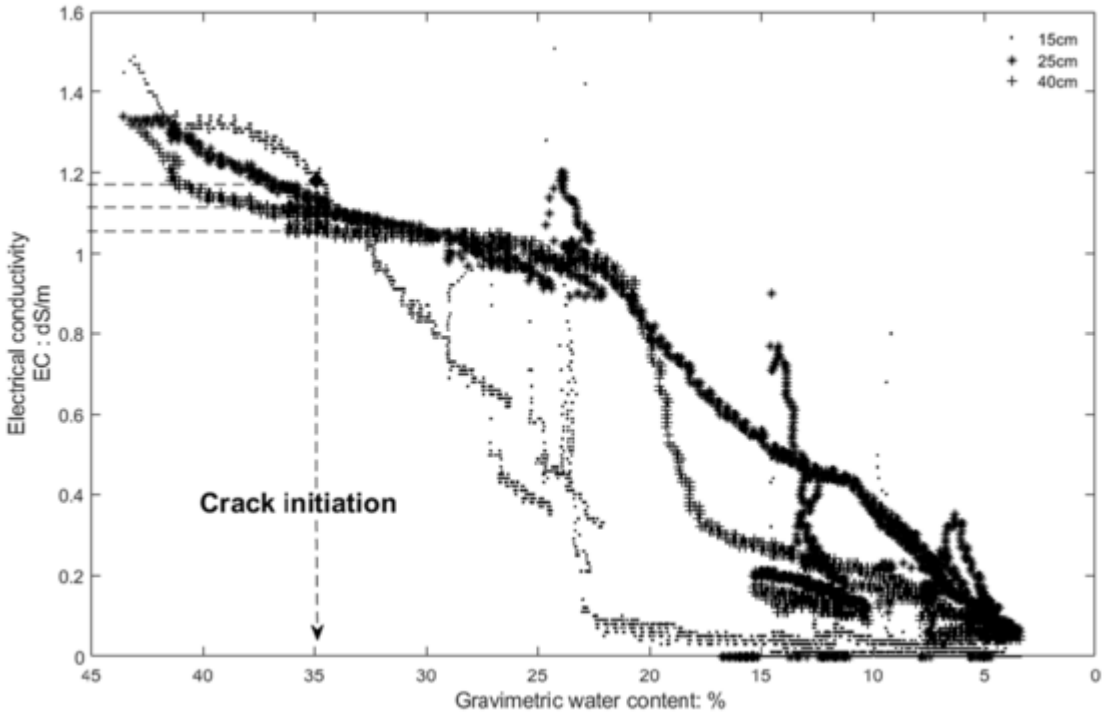

Fig. 18. Electrical conductivity in terms of the global gravimetric water content.

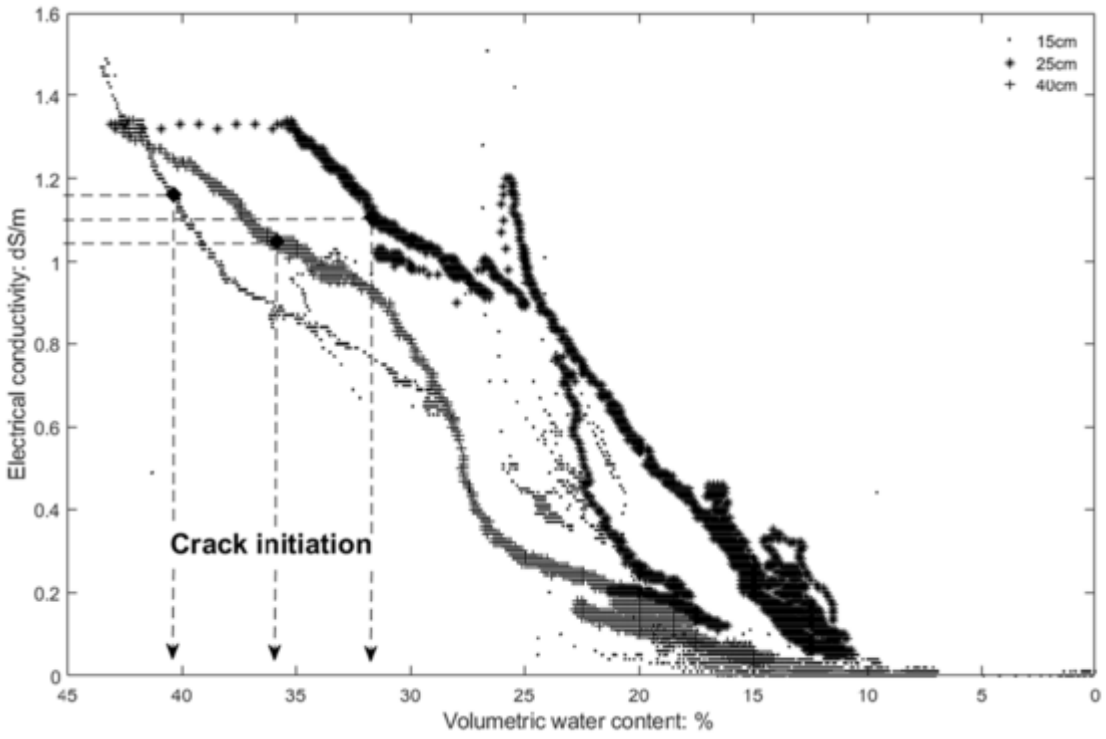

Fig. 19. Electrical conductivity in terms of the locally measured volumetric water content from sensors T1, T2 and T3.

3.4. Energy terms

Soil cracking is largely an effect of evaporation, a process which is dominated by energy and water availability. Therefore, all variables involved in the energy balance equation (which reflect daily and seasonal variations of energy flows) have an impact in the drying process and the cracking of the specimen.

In the case of the experiment reported in this paper, the global solar radiation is the main energy source. Therefore, it is necessary to distinguish between overcast and clear days. In overcast days (e.g., 2015-01-19) the global solar radiation value is low (Fig. 20a) and corresponds to a very uniform temperature profile (Fig. 20b). In clear days (e.g., 2015-01-18) temperature in the air shows more fluctuations than in the soil specimen but the temperature on the soil surface follows similar trends as the air temperature (Fig. 20b).

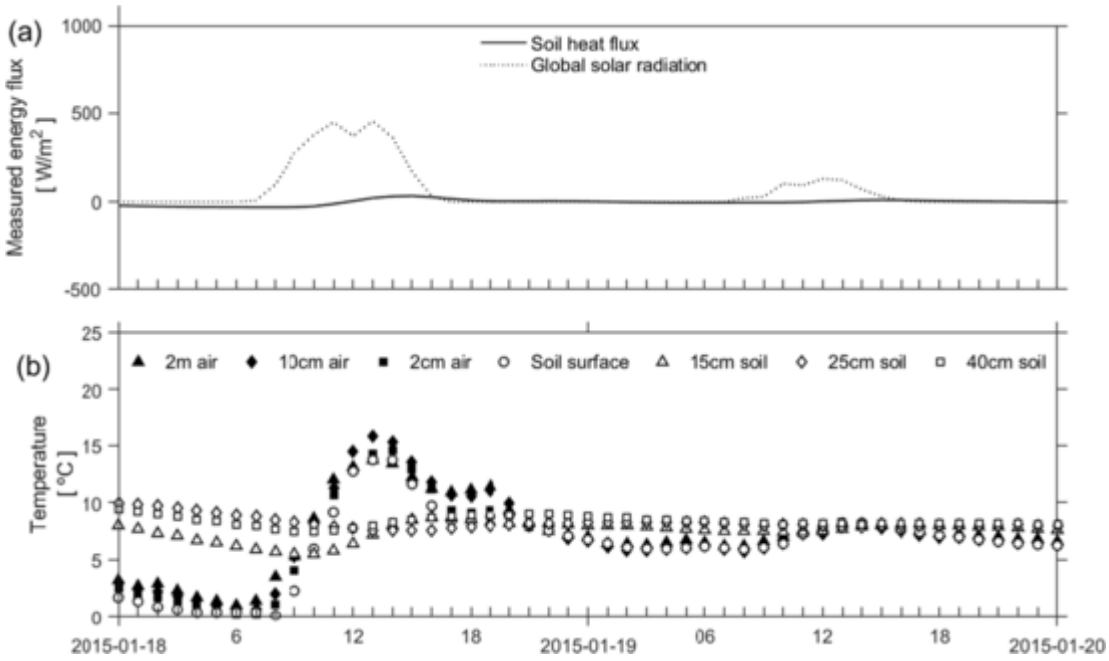

Fig. 20. Clear (2015-01-18) and overcast (2015-01-19) days: (a) energy (positive means into the ground); (b) air and soil temperatures.

Temperature profiles at different times of three particular days plotted in Fig. 21 manifest low gradients for overcast days in contrast to clear days in winter, which exhibits daily fluctuations at sunrise (7 am), mid-day and sunset (5 pm). Temperature follows daily fluctuations in which the soil specimen is colder at sunrise (see Fig. 21a), causing a negative heat flow (ground to air); it also becomes negative at sunset (see Fig. 21c), but the temperature diminishes more gradually compared to early morning. During the day the heat flow is positive (air to ground) with temperatures decreasing with depth. These fluctuations of the energy flow reflect the capacity of the soil to store and release energy through various processes in the interaction with the atmosphere.

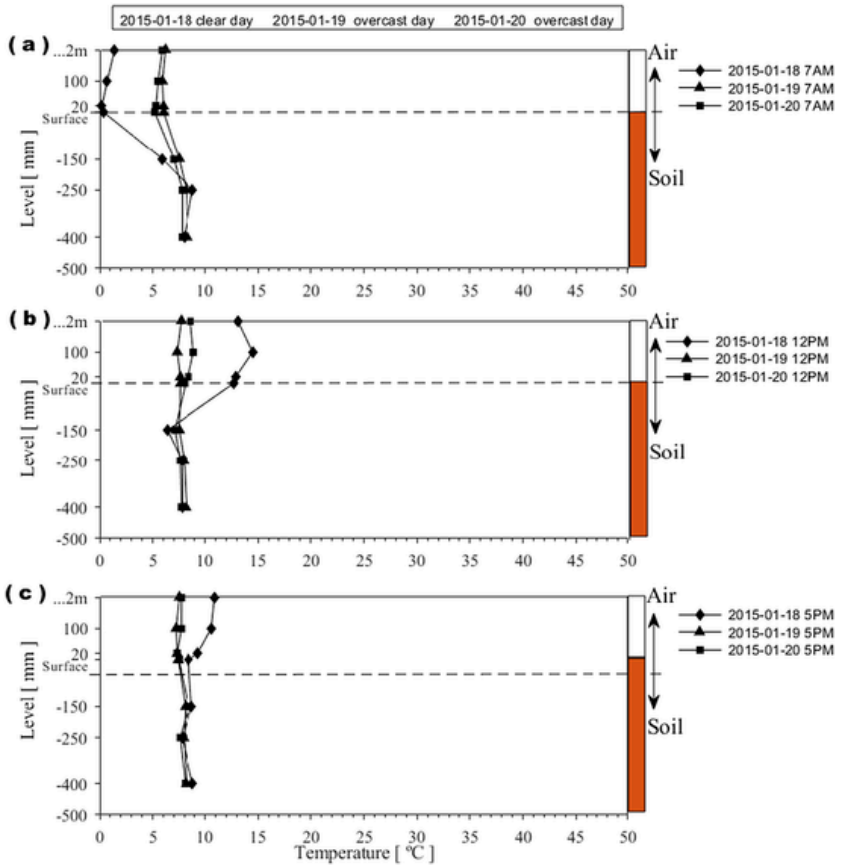

Fig. 21. Temperature profiles above and below the soil surface on the first three days of the test at three different times: a) 7 am, b) noon, c) 5 pm.

Temperature and solar radiation vary considerably throughout the annual cycle. The global solar radiation shows peaks around noon, as expected, with values much higher during spring and summer. The heat flow trend follows the solar global radiation trend but with negative values (ground to air) and a slight delay, being always a negligible part of the source of energy. When the temperature of the atmosphere is higher than the temperature at the specimen's surface, there is a sensible heat flow into the soil. Measurements taken in the upper layer near the surface show higher temperatures, as expected.

The soil temperature near the surface was colder than the atmosphere's during the day, while the opposite occurred during the night. The temperature measured below a depth of 25 cm was relatively constant and slightly higher because the heat stored in the soil.

In winter and autumn, the soil surface temperature increased only slightly as a consequence of the low solar radiation. The air temperature was higher than the specimen's during the day, with a negative sensible heat flow from air to ground, which may represent an additional source of energy for the system in wet periods. Particularly in winter, when the water content in the specimen was higher, the atmospheric demand for soil water with the supplied energy could be satisfied. On the other hand, in drier periods, the specimen was no longer able to meet this demand fully, and a part of the energy provided converted into sensible heat flux.

In spring and summer, the higher solar radiation contributed to increase the soil surface temperature, which was almost always higher than the air temperature. The thermal inertia of the soil was smaller when the soil was drier; then the oscillations of the temperature difference between soil and air were larger than with a wet soil, with the soil temperature always higher than the air's, and a positive sensible heat flow from ground to air.

Figs. 22 and 23 show the daily variation of the water volume influx (volume of water entering the soil minus water leaving the soil per unit surface area and time) and the wind speed during two selected windy days (2015-02-22 and 2015-02-25) with peaks of wind velocity at noon and 8 am when the solar radiations were 693 W/m^2 and 244 W/m^2, respectively. Both figures show that the minimum volume influx (indicating maximum evaporation) occurs mostly during hours with solar radiation.

The peaks of wind velocity usually coincide with periods of low air relative humidity and high values of evaporation (negative volume influx). During periods of low wind velocity (< 1 m/s) and without solar radiation, there is no noticeable evaporation, or even there is a gain of water mass (positive volume influx). Fig. 22 exhibits the maximum hourly evaporation (approximately −1.5 mm/h of volume influx) at noon, coinciding with the peak wind velocity and higher solar radiation. Fig. 23 displays the maximum daily evaporation (the minimum volume influx) at 8 am, also coinciding with the peak wind velocity, although in this case the global solar radiation was low.

Fig. 24 shows the air relative humidity and wind speed at different heights, and the volume influx, on 2015-05-24, when the gravimetric moisture content was approximately 10%, and the wind speed had a steady trend of less than 2 m/s throughout the day, which seems to have a smaller effect on evaporation. The higher evaporation during that day occurred mostly at times when the relative humidity was at its lowest.

Evaporation represents a loss of the water mass in the soil that results in a negative volume influx. It is the main atmospheric action linking the water and energy cycles. The energy spent in evaporating water from the soil surface depends mostly on temperature gradients from radiative energy flows. Therefore, the energy controls the transfer of water between soil and atmosphere. High evaporation rates dry the soil's surface, thus inducing shrinkage that may trigger crack initiation in the soil mass.

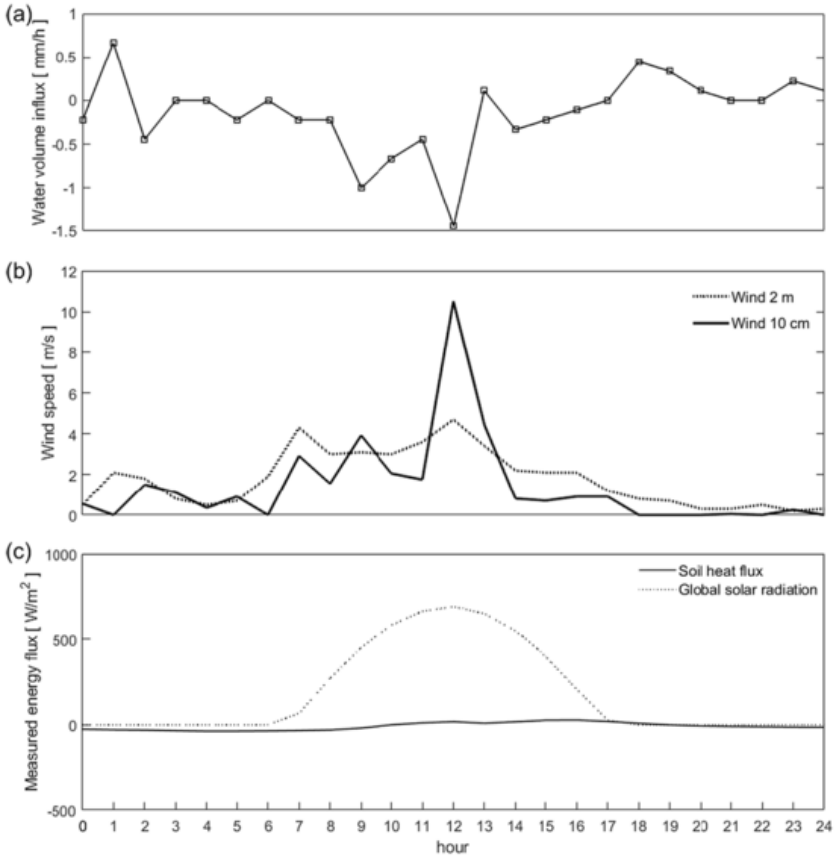

Fig. 22. Daily variation on 2015-02-22 of (a) water volume influx; (b) wind speed at two heights above soil surface; (c) Soil heat flux and solar radiation.

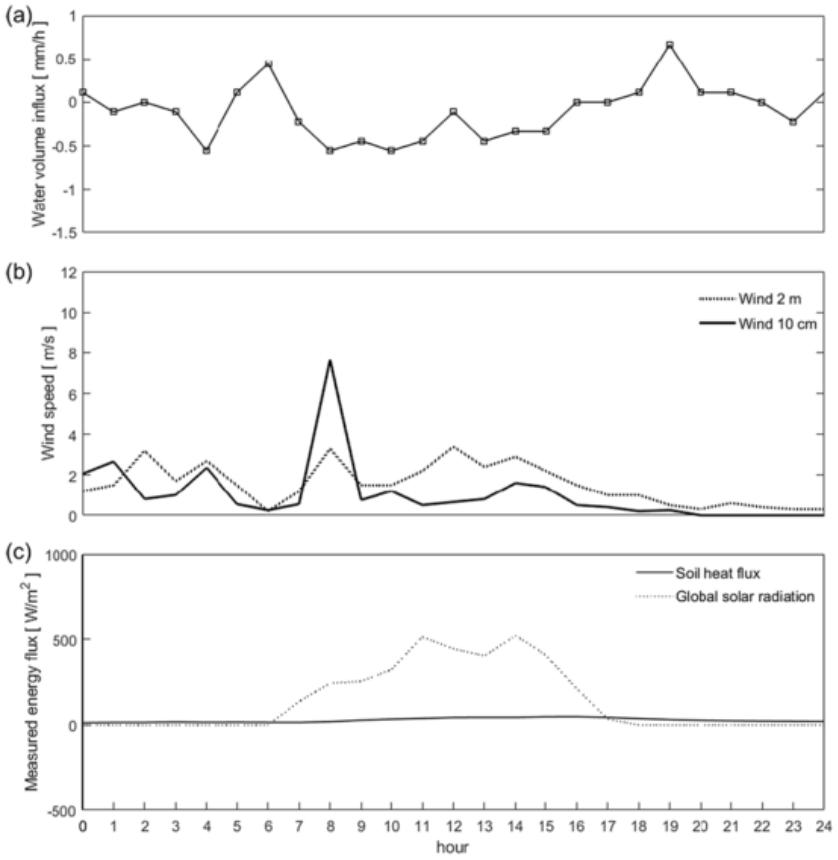

Fig. 23. Daily variation on 2015-02-25 of (a) water volume influx; (b) wind speed at two heights above soil surface; (c) soil heat flux and solar radiation.

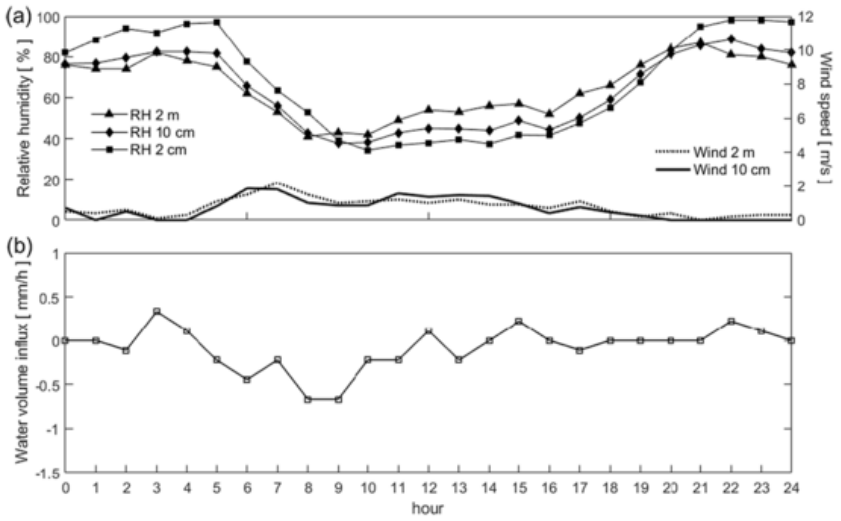

Fig. 24. Daily variation on 2015-05-24 of (a) air relative humidity/wind speed at different heights; (b) water volume influx.

Figs. 25 and 26 show variables related to the soil water and energy flow, such as volume influx, heat flow, global solar radiation, wind speed at 10 cm above the surface, relative humidity and air temperature at 2 cm above the surface, at three different hours, including sunrise and sunset (07:00 and 17:00 UTC, respectively) in winter, with low radiation, and at noon, with high radiation.

It is very difficult to analyse the individual effect of each environmental variable (solar radiation, relative humidity, temperature, wind velocity), as they are thermodynamically related in a nonlinear manner (Lozada et al., 2019). Periods of high solar radiation coincide with periods of low water volume influx, although the rest of variables may contribute to the evaporation as well. However, when the radiation is very low, the effect of wind velocity becomes particularly important. Before the onset of cracking (Fig. 25), there was no evaporation in the hours with low radiation (triangle markers). After cracks began to form (Fig. 26), in some days with high wind speed (such as days 24, 27, 30) evaporation (negative volume influx) happened even with low radiation, demonstrating the importance of considering the wind velocity in the desiccation process. Increments of wind speed seem to coincide with low values of relative humidity above the soil because wind removes wet air and heat, thus explaining temperature gradients close to the soil surface.

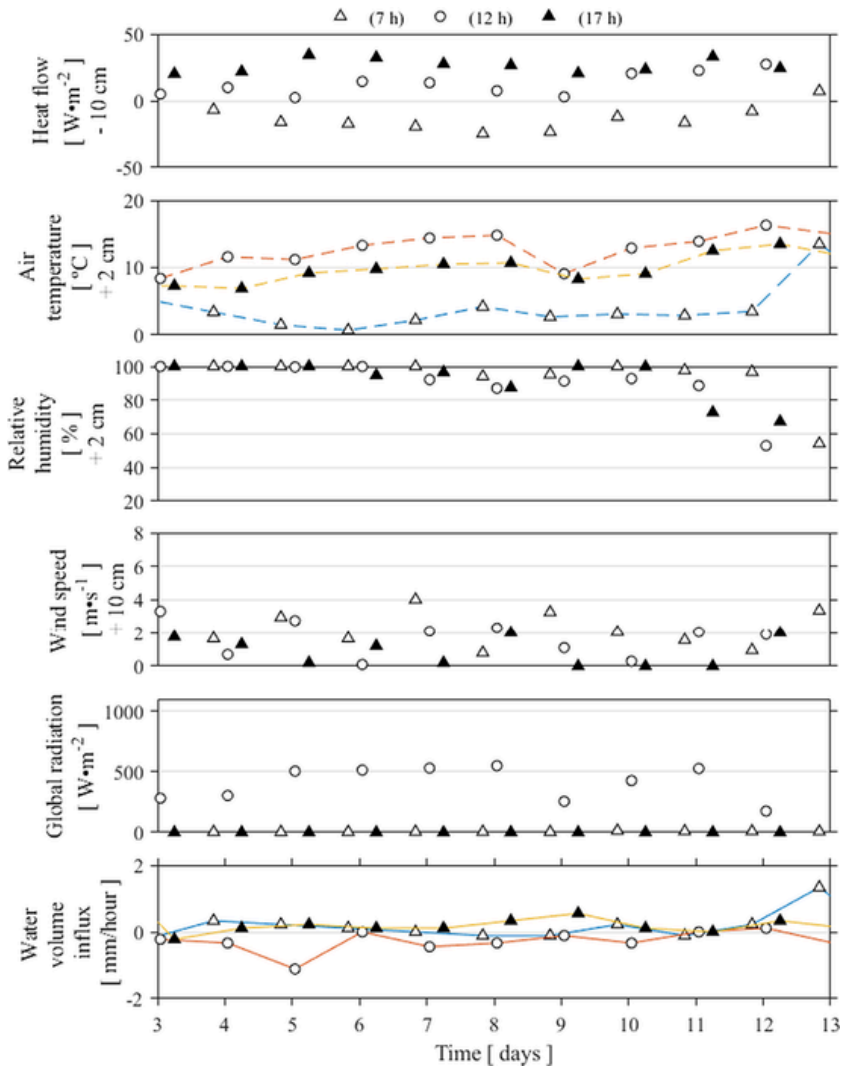

Fig. 25. Atmospheric variables and water volume influx at three different times during the second dry period (before the onset of cracking).

At sunrise (Figs. 25-26, hollow triangles) solar radiation was generally low or negligible and the energy flow was from soil to atmosphere, with the soil becoming cooler. This is consistent with negative heat flow values in the soil. However, at sunset (Figs. 25-26, solid triangles), although the solar radiation was also low, the heat flow in the soil was positive, occasionally exceeding the values at noon (Figs. 25-26, hollow circles).

When analysing Figs. 25 and 26, there are two visible effects to highlight: one is the effect of radiation on the daily fluctuation of the energy to and from the soil specimen. The other is that, with the presence of the water film at the beginning of the test, there was a high soil heat flux at sunset (compared to the heat flux at noon), which seems to be related to the capacity of water to store more energy.

4. Conclusions

The paper describes an experiment conducted on a large-scale soil specimen exposed during a one-year period to real atmospheric conditions with extensive instrumentation measuring relevant variables of soil, air, and the soil-air interface zone.

The results of the monitored physical variables allow explaining the desiccation process and to study the influence of environmental conditions in the soil cracks. The results show daily day/night fluctuations of the air temperature and the global solar radiation. Likewise, the annual seasonal variations have contributed to the development of the soil desiccation cracks. Rainfall events may affect the cracking patterns as well, which also change with time.

Because initially the soil used in the test had a very liquid consistency, the solid particles settled by gravity and the water moved vertically toward the surface, forming a water film and increasing the moisture content near the surface. At the initial conditions, with the soil saturated, narrow cracks of millimetric thickness appeared randomly at locations governed by the prevalent heterogeneity near the container walls, but they faded as the water began to accumulate at the specimen's surface. Permanent cracks began forming at day 22 during the third dry-wet cycle when a thin water film still remained on the surface at the corners of the container indicating that the specimen was mostly saturated.

The changes of the volumetric water content were faster during winter, when the test started and the less dense soil structure had more water availability. Suction started increasing sharply after the first month of the test when the CIF had reached more than 5%. Suction decreased with depth, with the values near the soil surface being the highest. The MPS6 sensors used to measure the suction stopped when they were exposed to the open atmosphere due to the cracks, reaching their measurement limit at the beginning of summer. The simultaneous measurements of suction and volumetric water content provide data to determine the soil water retention curve at multiple depths. The difference among curves can be attributed to porosity changes during the desiccation process.

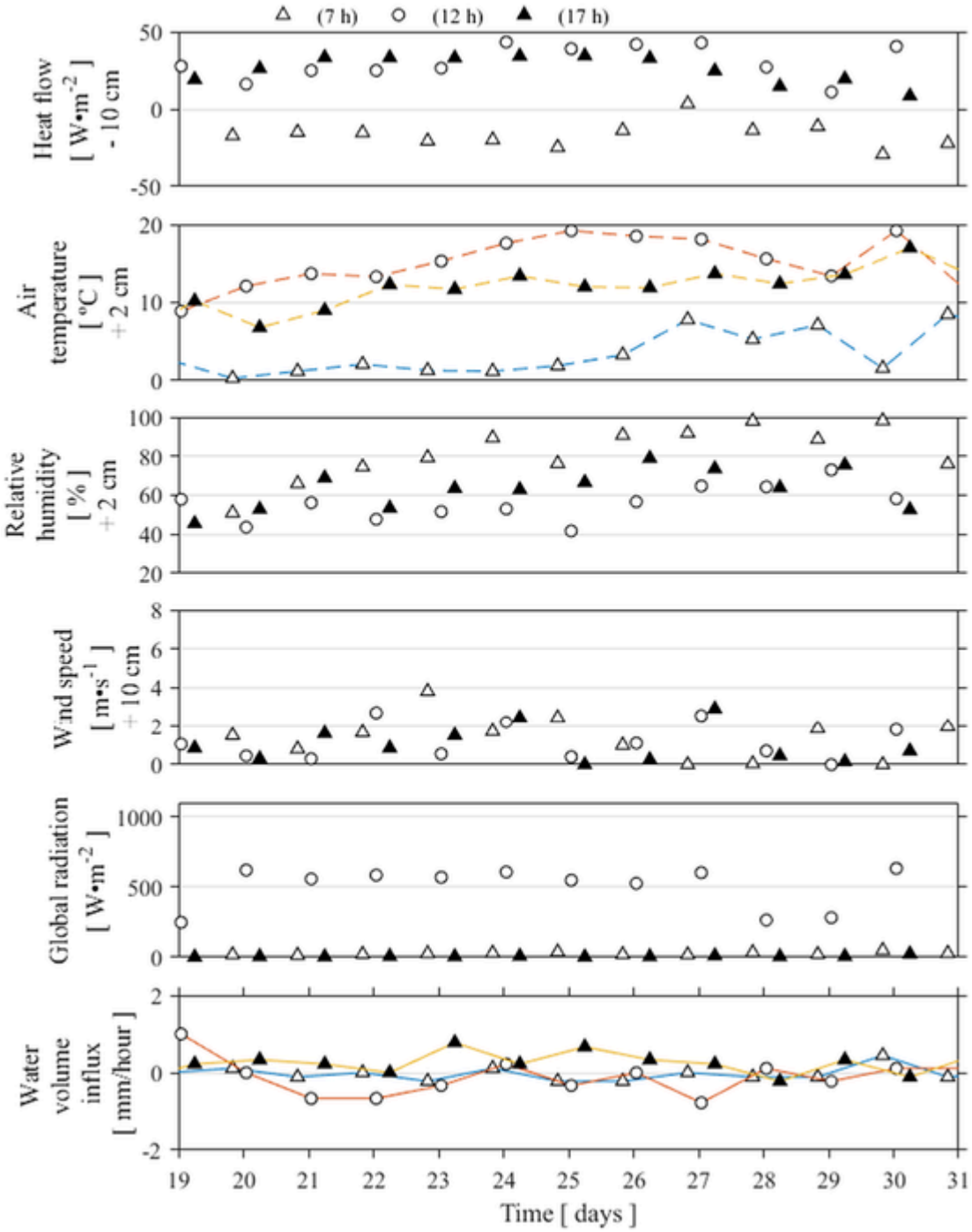

Fig. 26. Atmospheric variables and water volume influx at three different times during the third dry period (crack onset on day 22).

During desiccating processes, electrical conductivity may change with water content. As the soil dries, the values decrease because of the salts left by the evaporating water and the corresponding loss of ion mobility, showing that the electrical conductivity in the soil varies with the water content. The crack depth and the number of cracks also affect the evolution of the electrical conductivity.

At high solar radiation values (around mid-day hours) the soil temperature was colder than those in the air even with an established crack pattern. Despite of the drier state of the soil diminishing the thermal inertia and making a denser moist crack air, it seems that the effect of cracks was negligible on the heat fluxes, according to the measurements obtained in the experiment. Soils act as a repository of heat, gaining heat during day/warm months and losing heat during night/cold months. In addition to that, cracks do not change substantially the evaporation rate.

The results revealed that the negative water volume influx values (evaporation) correspond mostly to high solar radiation periods or, alternatively, to periods with low solar radiation but with high wind velocity. Therefore, the effect of wind velocity is more significant in hours with low solar radiation. Increments of wind speed seem to coincide with low values of relative humidity above the soil because wind removes moist air and heat, thus explaining the high temperature gradients close to the soil surface.

The onset of crack initiation adjusts well with the decreasing of volumetric water content in the upper layer of the specimen. However, the increment of the measured suction lags several days relative to the start

of the water loss process. Due to rainfall-induced flooding, the CIF increased because the more significant cracks became wider. As a consequence, in the following dry period, the CIF decreased because the edges of the larger cracks collapsed, resulting in loose material filling in the existing cracks.

The experiment extends the previous experience from laboratory desiccating tests, including solar radiation and wind in natural conditions, which constitute two key factors controlling water evaporation and eventually soil cracking. The soil-air interface constitutes a narrow zone with high gradients of most of the variables involved and it controls the fluxes of water and energy. The experiment has shown the variation of those gradients and the implications in soil cracking.

Funding

This work was supported by the Spanish Ministry of Economy and Competitiveness (grant BIA2012-36498) and the Spanish Ministry of Science, Innovation and Universities (grant BIA2017-82594-R) both including FEDER funds from the European Commission.

CRediT authorship contribution statement

Josbel A. Cordero: Methodology, Formal analysis, Investigation, Writing - original draft, Writing - review & editing, Visualization. **Pere C. Prat:** Conceptualization, Methodology, Resources, Writing - original draft, Writing - review & editing, Supervision, Project administration, Funding acquisition. **Alberto Ledesma:** Conceptualization, Methodology, Validation, Resources, Writing - original draft, Writing - review & editing, Supervision, Funding acquisition.

Declaration of Competing Interest

The authors declare that they have no known competing financial interests or personal relationships that could have appeared to influence the work reported in this paper.

Acknowledgements

The authors wish to thank Miquel Masip and Geralds Useche for their help in the long and tedious process of preparation of the field test.

References

Alonso-Arroyo, A., Torrecilla, S., Querol, J., Camps, A., Pascual, D., Park, H., Onrubia, R., 2015. Two dedicated soil moisture experiments using the scatterometric properties of GNSS-reflectometry. In: International Geoscience and Remote Sensing Symposium (IGARSS). pp. 3921–3924.

Amarasiri, A.L., Kodikara, J., Costa, S., 2011. Numerical modelling of desiccation cracking. Int. J. Numer. Anal. Methods Geomech. 35, 82–96. https://doi.org/10.1002/nag.894.

Blight, G.E., 1997. Interactions between the atmosphere and the Earth. Géotechnique 47, 713–767. https://doi.org/10.1680/geot.1997.47.4.713.

Bonin, M.D., Cabral, A.R., Nuth, M., 2019. Examination of the effects of solids content on thickened gold mine tailings sedimentation and self-weight consolidation. Geotech. Test. J. 42, 1493–1517. https://doi.org/10.1520/GTJ20180094.

Chertkov, V.Y., 2002. Modelling cracking stages of saturated soils as they dry and shrink. Eur. J. Soil Sci. 53, 105–118. https://doi.org/10.1046/j.1365-2389.2002.00430.x.

Cordero, J., 2019. Experimental Analysis of Soil Cracking due to Environmental Conditions Ph.D. Thesis UPC-BarcelonaTech.

Cordero, J., Cuadrado, A., Prat, P.C., Ledesma, A., 2016. Description of a field test involving cracking in a drying soil. In: 3rd European Conference on Unsaturated Soils – E-UNSAT 2016. E3S Web of Conferences 9, 12005. pp. 1–6 Paris.

Cordero, J., Useche, G., Prat, P.C., Ledesma, A., Santamarina, J.C., 2017. Soil desiccation cracks as a suction-contraction effect. Géotech. Lett. 7, 272–278. https://doi.org/10.1680/jgele.17.00070.

Corte, A., Higashi, A., 1960. Experimental research on desiccation cracks in soil. In: US Army Snow, Ice and Permafrost Research Establishment Report. p. 66.

Costa, S., Kodikara, J., Shannon, B., 2013. Salient factors controlling desiccation cracking of clay in laboratory experiments. Géotechnique 63, 18–29. https://doi.org/10.1680/geot.9.P.105.

Cuadrado, A., 2019. THM Analysis of the Soil-atmosphere Interaction in Clay Soils Under Drying Conditions (in Spanish) Ph.D. Thesis UPC-BarcelonaTech.

Cuadrado, A., Encalada, D., Ledesma, A., Prat, P.C., 2019. Soil surface boundary condition in desiccating soils. In: Sigursteinsson, H., Erlingsson, S., Bessason, B. (Eds.), XVII European Soil Mechanics and Geotechnical Engineering Conference. Jarðtæknifélag Íslands / Icelandic Geotechnical Society, Reykjavík, Iceland.

Cuadrado, A., Najdi, A., Ledesma, A., Olivella, S., Prat, P.C., 2021. THM Analysis of a Soil Drying Test in an Environmental Chamber: The Role of Boundary Conditions Report Dept. of Civil and Environmental Engineering, UPC-BarcelonaTECH.

Cui, Y.J., Lu, Y.F., Delage, P., Riffard, M., 2005. Field simulation of in situ water content and temperature changes due to ground atmospheric interactions. Géotechnique 55, 557–567. https://doi.org/10.1680/geot.2005.55.7.557.

Cui, Y.J., Ta, A.N., Hemmati, S., Tang, A.-M., Gatmiri, B., 2013. Experimental and numerical investigation of soil-atmosphere interaction. Eng. Geol. 165, 20–28. https://doi.org/10.1016/j.enggeo.2012.03.018.

Davarzani, H., Smits, K., Tolene, R.M., Illangasekare, T.H., 2014. Study of the effect of wind speed on evaporation from soil through integrated modeling of the atmospheric boundary layer and shallow subsurface. Water Resour. Res. 50. https://doi.org/10.1002/2013WR013952.

DecagonDevices, 2015. VP-3 Vapor Pressure, Temperature & Relative Humidity Sensor Operator's Manual. Decagon Devices, Inc, Pullman WA, p. 99163.

Gui, Y., Zhao, G.F., 2015. Modelling of laboratory soil desiccation cracking using DLSM with a two-phase bond model. Comput. Geotech. 69, 578–587. https://doi.org/10.1016/j.compgeo.2015.07.001.

Harris, R., 2004. Giant desiccation cracks. In: Open File Report, OFR-04-01, Arizona Geological Survey.

Kodikara, J.K., Nahlawi, H., Bouazza, A., 2004. Modelling of curling in desiccation clay. Can. Geotech. J. 41, 560–566. https://doi.org/10.1139/t04-015.

Kong, L.W., Bai, W., Guo, A.G., 2012. Effects of cracks on the electrical conductivity of a fissured laterite: a combined experimental and statistical study. Geotech. Test. J. 35, 1–9. https://doi.org/10.1520/GTJ20120070.

Konrad, J.-M., Ayad, R., 1997. Desiccation of a sensitive clay: field experimental observations. Can. Geotech. J. 34, 929–942. https://doi.org/10.1139/t97-063.

Lakshmikantha, M.R., 2009. Experimental and Theoretical Analysis of Cracking in Drying Soils Ph.D. Thesis UPC-BarcelonaTech.

Lakshmikantha, M.R., Prat, P.C., Ledesma, A., 2009. Image analysis for the quantification of a developing crack network on a drying soil. Geotech. Test. J. 32, 505–515. https://doi.org/10.1520/GTJ102216.

Lakshmikantha, M.R., Prat, P.C., Ledesma, A., 2012. Experimental evidences of size-effect in soil cracking. Can. Geotech. J. 49, 264–284. https://doi.org/10.1139/T11-102.

Lakshmikantha, M.R., Prat, P.C., Ledesma, A., 2018. Boundary effects in the desiccation of soil layers with controlled environmental conditions. Geotech. Test. J. 41, 675–697. https://doi.org/10.1520/GTJ20170018.

Ledesma, A., 2016. Cracking in desiccating soils. In: 3rd European Conference on Unsaturated Soils – E-UNSAT 2016. E3S Web of Conferences 9, 03005, Paris. pp. 1–8.

Levatti, H.U., 2015. Experimental Study and Numerical Analysis of Drying in Clayey Soils (in Spanish) Ph.D. Thesis UPC-BarcelonaTech.

Levatti, H.U., Prat, P.C., Ledesma, A., Cuadrado, A., Cordero, J., 2017. Experimental analysis of 3D cracking in drying soils using Ground Penetrating Radar. Geotech. Test. J. 40, 221–243. https://doi.org/10.1520/GTJ20160066.

Levatti, H.U., Prat, P.C., Ledesma, A., 2019. Numerical and experimental study of initiation and propagation of desiccation cracks in clayey soils. Comput. Geotech. 105, 155–167. https://doi.org/10.1016/j.compgeo.2018.09.015.

Li, J.H., Zhang, L.M., 2011. Study of desiccation crack initiation and development at ground surface. Eng. Geol. 123, 347–358. https://doi.org/10.1016/j.enggeo.2011.09.015.

Lozada, C., Caicedo, B., Thorel, L., 2019. A new climatic chamber for studying soil–atmosphere interaction in physical models. Int. J. Phys. Model. Geotech. 19, 286–304. https://doi.org/10.1680/jphmg.17.00073.

Miller, C.J., Mi, H., Yesiller, N., 1998. Experimental analysis of desiccation crack propagation in clay liners. J. Am. Water Resour. Assoc. 34, 677–686. https://doi.org/10.1111/j.1752-1688.1998.tb00964.x.

Nahlawi, H., Kodikara, J., 2006. Laboratory experiments on desiccation cracking of thin soil layers. Geotech. Geol. Eng. 24, 1641–1664. https://doi.org/10.1007/s10706-005-4894-4.

Neal, J.T., Langer, A.M., Kerr, P.F., 1968. Giant desiccation polygons of great basin playas. Bull. Geol. Soc. Am. 79, 69–90. https://doi.org/10.1130/0016-7606(1968)79[69:GDPOGB]2.0.CO;2.

Péron, H., Hueckel, T., Laloui, L., Hu, L.B., 2009. Fundamentals of desiccation cracking of fine-grained soils: experimental characterisation and mechanisms identification. Can. Geotech. J. 46, 1177–1201. https://doi.org/10.1139/T09-054.

Rodríguez, R.L., Sánchez, M.J., Ledesma, A., Lloret, A., 2007. Experimental and numerical analysis of a mining waste desiccation. Can. Geotech. J. 44, 644–658. https://doi.org/10.1139/T07-016.

Sánchez, M., Atique, A., Kim, S., Romero, E., Zielinski, M., 2013. Exploring desiccation cracks in soils using a 2D profile laser device. Acta Geotech. 8, 583–596. https://doi.org/10.1007/s11440-013-0272-1.

Sánchez, M., Manzoli, O.L., Guimarães, L.N., 2014. Modeling 3-D desiccation soil crack networks using a mesh fragmentation technique. Comput. Geotech. 62, 27–39. https://doi.org/10.1016/j.compgeo.2014.06.009.

Shin, H., Santamarina, J.C., 2011. Desiccation cracks in saturated fine-grained soils: particle-level phenomena and effective-stress analysis. Géotechnique 61, 961–972. https://doi.org/10.1680/geot.8.P.012.

Shokri, N., Zhou, P., Keshmiri, A., 2015. Patterns of desiccation cracks in saline bentonite layers. Transp. Porous Media 110, 333–344. https://doi.org/10.1007/s11242-015-0521-x.

Song, W.-K., 2014. Experimental Investigation of Water Evaporation From Sand and Clay Using an Environmental Chamber Ph.D. Thesis Université Paris-Est.
Song, W.-K., Cui, Y.-J., Tang, A.M., Ding, W.-Q., Wang, Q., 2016. Experimental study on water evaporation from compacted clay using environmental chamber. Can. Geotech. J. 53, 1293–1304. https://doi.org/10.1139/cgj-2015-0415.
Stirling, R.A., Glendinning, S., Davie, C.T., 2017. Modelling the deterioration of the near surface caused by drying induced cracking. Appl. Clay Sci. 146, 176–185. https://doi.org/10.1016/j.clay.2017.06.003.
Stirling, R.A., Glendinning, S., Davie, C.T., Hen-Jones, R., Hughes, P.N., 2018. The behaviour and influence of desiccation cracking on a full-scale, vegetated infrastructure embankment. In: Ng, C.W.W., Leung, A.K., Chiu, A.C.F., Zhou, C. (Eds.), 7th International Conference on Unsaturated Soils (UNSAT2018). HKUST, Hong Kong.
Stirling, R.A., Toll, D.G., Glendinning, S., Helm, P.R., Yildiz, A., Hughes, P.N., Asquith, J. D., 2020. Weather-driven deterioration processes affecting the performance of embankment slopes. Géotechnique 1–43. https://doi.org/10.1680/jgeot.19.sip.038.
Tang, C.-S., Shi, B., Liu, C., Suo, W.-B., Gao, L., 2011. Experimental characterization of shrinkage and desiccation cracking in thin clay layer. Appl. Clay Sci. 52, 69–77. https://doi.org/10.1016/j.clay.2011.01.032.
Tang, C.-S., Cheng, Q., Leng, T., Shi, B., Zeng, H., Inyang, H.I., 2020. Effects of wetting-drying cycles and desiccation cracks on mechanical behavior of an unsaturated soil. CATENA 194, 104721. https://doi.org/10.1016/j.catena.2020.104721.
Tollenaar, R.N., van Paassen, L.A., Jommi, C., 2018. Small-scale evaporation tests on clay: influence of drying rate on clayey soil layer. Can. Geotech. J. 55, 437–445. https://doi.org/10.1139/cgj-2017-0061.
Trabelsi, H., Jamei, M., Zenzri, H., Olivella, S., 2012. Crack patterns in clayey soils: experiments and modeling. Int. J. Numer. Anal. Methods Geomech. 36, 1410–1433. https://doi.org/10.1002/nag.1060.
Tristancho, J., Caicedo, B., Thorel, L., Obregón, N., 2012. Climatic chamber with centrifuge to simulate different weather conditions. Geotech. Test. J. 35, 159–171. https://doi.org/10.1520/GTJ103620.
Wang, L.-L., Tang, C.-S., Shi, B., Cui, Y.J., Zhang, G.-Q., Hilary, I., 2018. Nucleation and propagation mechanisms of soil desiccation cracks. Eng. Geol. 238, 27–35. https://doi.org/10.1016/j.enggeo.2018.03.004.
Yamanaka, T., Takeda, A., Sugita, F., 1997. A modified surface-resistance approach for representing bare-soil evaporation: Wind tunnel experiments under various atmospheric conditions. Water Resour. Res. 33, 2117–2128. https://doi.org/10.1029/97WR01639.
Yesiller, N., Miller, C.J., Inci, G., Yaldo, K., 2000. Desiccation and cracking behavior of three compacted landfill liner soils. Eng. Geol. 57, 105–121. https://doi.org/10.1016/S0013-7952(00)00022-3.
Yoshida, S., Adachi, K., 2004. Numerical analysis of crack generation in saturated deformable soil under row-planted vegetation. Geoderma 120, 63–74. https://doi.org/10.1016/j.geoderma.2003.08.009.
Yu, Z., Eminue, O.O., Stirling, R.A., Davie, C.T., Glendinning, S., 2021. Desiccation cracking at field scale on a vegetated infrastructure embankment. Géotech. Lett. 11, 1–21. https://doi.org/10.1680/jgele.20.00108.